Analytical Methods

ROYAL SOCIETY OF CHEMISTRY

CRITICAL REVIEW

View Article Online
View Journal | View Issue

Cite this: *Anal. Methods*, 2025, **17**, 916

Combining digital imaging and quantum dots for analytical purposes

João Paulo B. de Almeida,[a] Thomas Fernando Ferreira Tributino dos Santos,[a] José Roberto Sabino Júnior,[a] Elias Vinicius Ferreira do Amaral,[a] Claudinéia R. S. Oliveira,[b] Matheus V. Maia,[b] Willian T. Suarez,[b] Lucas B. Ayres,[c] Carlos D. Garcia[c] and Vagner B. dos Santos *[ac]

This review provides a critical assessment of the most recent advances in digital imaging (DI) methods, applied for the development of analytical methodologies combining quantum dots (QDs). The state-of-the-art, treatment of data, instrumental considerations, software, sensing approaches, and optimization of the resulting methods are reported. Applications of the technology for the analysis of food and beverages, biomedically relevant analytes, drugs, environmental samples and forensic samples are also discussed. These examples aim to highlight the advantages of DI over traditional instrumentation, that in combination with QDs represents a powerful option for low-cost and on-site analyses. Moreover, some of these DI methods have been explored in the context of green chemistry principles, demonstrating a sustainable approach to modern analytical challenges.

Received 18th November 2024
Accepted 19th December 2024

DOI: 10.1039/d4ay02097a

rsc.li/methods

1. Introduction

The advances in electronic devices observed in the last decade (especially in the field of smartphones) have allowed a significant growth in the number of analytical methods that take advantage of their high portability, accessibility, and high connectivity.[1,2] In fact, these modern analytical methods have been applied to address issues in medicine,[3,4] clinical,[4–7] forensics,[8] pharmaceutical,[9] environmental,[10,11] agricultural,[12] and food science,[13–15] among other fields.[16,17] One of the main advantages of these analytical methods is their intrinsic portability, leading to the possibility of not only performing the analysis on-site but also making decisions in real time.[18] While a variety of techniques have been widely used to create sensing platforms coupled to smartphones,[19,20] the present review is focused on optical methods based on the combination of digital imaging (DI) with quantum dots (QDs), which only require minimum accessories[2] for their implementation, besides the smartphone itself. These advantages have brought about an exponential increase in the number of publications linked to DI-QDs (Fig. 1), reaching almost 600 papers per year in the last few years.

Considering these aspects, this review aims to describe some of the most important contributions to this area, including developments in instrumentation[21] and software, the possibility of coupling machine learning models to provide fast response for DI-based methods,[22,23] and the incipient use of natural deep eutectic solvents.[13,24–27] These approaches are based on colorimetry, photometry/spectrometry,[28] or fluorimetry[29] and have targeted a wide variety of analytes (*e.g.* antibiotics,[1] glucose,[30]

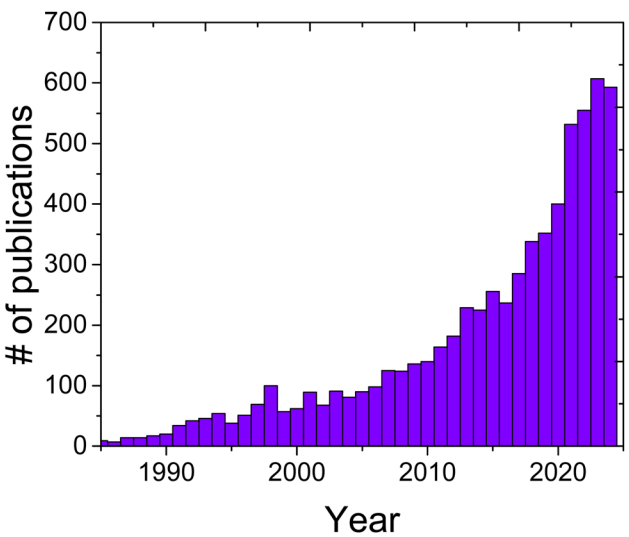

Fig. 1 Trend in the number of publications related to DI-QDs from 1985 to 2024 (November). Data obtained from the Web of Science using digital image and chemistry as keywords.

[a]*Department of Fundamental Chemistry, LIA[3] – Applied Analytical Instrumentation Laboratory, Federal University of Pernambuco, Av. Jornalista Anibal Fernandes, s/n, Cidade Universitária, Recife, PE, 50740-560, Brazil. E-mail: vagner.bsantos@ufpe.br*

[b]*Department of Chemistry, Federal University of Viçosa – UFV, Centro de Ciências Exatas e Tecnologia, Viçosa, MG, Brazil*

[c]*Department of Chemistry, Clemson University, 211 S. Palmetto Blvd, Clemson, SC 29634, USA*

melamine,[31] metallic ions,[32] toxic metals,[33] and biogenic amines[34]). It is also important to note that many of these methods have been developed together with paper sensors,[35–37] cotton,[38] metal–organic frameworks (MOFs),[39] and molecularly imprinted polymers (MIPs), or nanostructures.[40,41] These strategies allowed DI methods to increase their selectivity and sensitivity, enabling the analysis of more complex samples.[40,41] Among those, we focus on the use of DI with quantum dots (QDs),[42–46] which present unique optical properties and have already been used in photovoltaic cells,[47] light emitting diodes,[29] bioimaging,[48,49] and a wide range of analytical applications.[42,44]

2. Digital imaging methods

Although the first examples of digital imaging methods were presented by Epperson,[50] Maleki,[51] and Gaiao,[52] many other groups have reported DI coupled with colorimetric reactions.[53–56] In most of these cases, smartphones are used to measure the color intensity of a sample upon being illuminated with homogeneous white light by either absorbance[57] or reflectance.[58–61] While there is an established relationship between reflectance and absorbance,[16,21,62,63] there are also relatively simple ways to determine contributions from each of these mechanisms.[64] It is thus important that authors distinguish these phenomena in order to avoid conceptual errors.[38,60,65] In general, if the digital device only captures a photograph of the substrate/sample to calculate color intensity (for instance, of a paper device[66,67]), then the signal generated is likely due to reflectance.[61,63] In fluorescence DI (FDI) methods, an image of the sample is typically captured in a black chamber upon excitation with a UV source.[20,68] Readers are encouraged to consult a recent review by Shen[69] for additional details.

The mathematical models used to decompose digital images for analytical purposes were developed for colorimetry; however, they can be used in fluorimetry.[33] Here, only small modifications to the setup are required,[2,34] mostly related to the use of UV radiation to excite fluorophores.[70] Classic fluorescence probes like quinine[70] and rhodamine[71] have been reported in the literature and have paved the way for new contributions based on quantum dots.[72–75]

2.1. Instrumentation and accessories

For DI methods, several digital devices are typically used, including webcams,[52,76] scanners,[77] traditional digital cameras,[78,79] hyperspectral cameras,[79,80] and (of course) smartphones.[14,28,46,63,81,82] Sometimes, methods based on DI employ small accessories to accommodate the sample,[63] to provide a uniform illumination,[28,63,81] or to avoid shadows.[21,83] These accessories should be produced using inert materials, to avoid unwanted reactions and sample contamination. While polystyrene microplates[12] are incompatible with organic solvents,[84] platforms based on specific polymers (such as polylactic acid (PLA)),[70] ceramics,[85] paper,[35,86] or quartz[87] have been used. Although specifically discussed elsewhere,[88–90] it is important to consider the tremendous impact of 3D printers in the development of these accessories.[2,9,70,91]

Because the digital image obtained needs homogeneous illumination, several authors have developed closed chambers ("boxes") that can diffuse the light and avoid external influences without the need of a dark room (unsuitable for *in situ* analysis).[92] These boxes typically improve the precision of the data collected, and thus, the quality of the analytical method.[70] Although standard black plastic boxes[21,62] can be used, custom boxes made with PLA,[2] paper,[12,60,93] or plexiglass,[20,94,95] have been reported. While these boxes are essential when employing conventional UV lamps as excitation sources,[31,74,96] most authors have opted for the use of UV-LED sources. In general, LEDs are more adequate radiation sources due to the low power consumption,[97] high stability, long lifetime, and the possibility of focusing their emission (due to their low beam angle).[19,21,62,70] Additional parts can also be used to control the intensity of the light, such as diffusers (made with acrylic,[12] Teflon,[27] or paper[61]), optical filters,[12,98] or small electronic circuits (such as potentiometers),[84] often implemented using Arduino.[99–102]

In this context, Benedetti *et al.*[21] developed a system that integrated a plastic box, a smartphone and a digital camera. Besides incorporating a potentiometer to control the light intensity, these authors included a 12 V/5000 mA h battery, providing portability. The LED chamber was used for colorimetric detection of ethanol in alcoholic drinks with a linear range from 1.0 to 20.0% v/v, with a LOD of 0.25%, providing results that were indistinguishable (at the 95% confidence level) from those obtained with a traditional UV-Vis instrument and enabling in-line monitoring and quality control. da Silva *et al.*[70] developed a fluorimeter for detection of quinine in beverages, requiring the use of a chamber and four 10 W UV-LEDs. This method was validated using a commercial fluorimeter and had an LOD of 6.9×10^{-8} mol L^{-1}, which is comparable to that of other portable systems.[103]

2.2. Smartphones and color models

Perhaps the great success of DI methods can be ascribed to the use of smartphones, where recent advances in both hardware and software have given them a performance that can be compared to that of some computers, with enough memory and storage capacity to perform multiple analyses.[43] It is important to note that these advances have also favored the reduction in size of the corresponding analytical systems, further supporting the development of portable methodologies.[33,59,84,93,104] Moreover, smartphones not only provide simplicity but also the ultimate option for making analytical procedures more environmentally benign and safer for humans.[97] According to the AGREE calculator, and unlike webcams,[76,105,106] scanners,[77,107] and traditional digital cameras,[62,78,108] a method using a smartphone[18,33,41,59,84,93,104,109] does not have any penalty because it is considered that the user will carry one regardless of the analytical task. As a core element of smartphones, an important aspect is that the resolution of the cameras included has also exponentially improved, now featuring multiple lenses, improved image processing, and even several AI-assisted

shooting modes.[23] As a point of reference, the first iPhone was released in 2007 and featured a single camera of just 2 MP, whereas the latest Google Pixel 8 Pro includes a 50 MP camera with a 5× optical zoom.[14,43,81] Smartphones use either Charge Coupled Devices (CCD) or Complementary Metal Oxide Semiconductor (CMOS) sensors as cameras.[110,111] Due to their faster processing speed and information transfer, CMOS cameras are the prevalent option in current models.[28,46] Both CCD and CMOS are monochromatic, but each photodiode is used to detect determinate photons in the visible spectrum. Most color cameras work by capturing only primary color (RGB) at each sensor, using the Bayer color filter array (CFA).[110–112] As expected, each color channel covers a give spectral region, where the RGB channels cover the range of 550–800 nm (R), 450–650 nm (G), and 400–550 nm (B), respectively.[113] Thus, and considering the number of possible variables to consider when obtaining digital images for analytical purposes, it is important to use the same device and consistent settings (imaging mode, filter, zoom, *etc.*) throughout the experiments. For specific applications where the selection of the color is critical, it is also recommended to consider a calibration step.[57] While most current devices can be used to develop analytical applications, Benedetti *et al.*[21] noted that devices with different resolutions result in methods with similar sensitivity but different precisions (the higher the resolution, the higher the precision).

To obtain analytical information from a digital image, several color systems can be used. In general, the color models consist of a 3D coordinate system, where the x, y and z axes represent the primary colors (Fig. 2). The color models more widely reported in the literature are RGB, CMYK, HSI, HSV,[54,115] and CIELAB,[116] with RGB being the most widely reported for imaging (CMY and CMYK are mostly used for printers[61]). The selection of the color model is important for analytical applications, as parameters like hue, saturation and brightness can increase the versatility of the approach.[61]

The RGB system is formed by three components x, y and z, where each of them represents the red (R), green (G) and blue (B) channels, with the space delimited by the three axes of a cube. Each channel ranges from 0 to 255, where the combination of the three channels generates 16.777.216 colors, fully covering the visible spectrum from 400 to 800 nm. The origin (0, 0, 0) of the coordinates is 100% black, while the coordinate (255, 255, 255) is 100% white.[115] In this model, the gray scale is equivalent to the point of equal RGB values for the three channels extending from black (0, 0, 0) to white (255, 255, 255) along the straight line linking these two points.[115,117,118] The other colors are represented by points located in the subspace delimited by the cube defined by vectors that extend from the origin.[76] Sometimes the RGB scale is normalized to values ranging from 0 to 1.[119] The CMY and CMYK color systems represent systems composed of the colors cyan, magenta, and yellow (CMY) and cyan, magenta, yellow and black (CMYK) as the main colors. The colors blue, green and red are classified as secondary colors in this system.[61,63,119] On the other hand, the HSV color model presents the components for hue (H), saturation (S) and value (brightness of a given color). Hue describes the color as degrees that represent the location on the standard color wheel.[61] Thus, hue is the main color property that allows us to distinguish between different colors. As an example, there is red with a value of 0°, yellow with 60°, green with 120°, blue with a value of 240°, *etc.* Saturation describes the intensity of a color ranging from 0 to 100%, with the higher value being the more intense the color. The brightness component describes the percentage of white in the color, with values varying from 0 to 100%.[115,119]

The color coordinates obtained after the decomposition of the digital image are then used as the signal or further processed. The former case is the most common and involves, for example, the use of the intensity of the B-channel (originating from the blue light emitted by a quantum dot)[2,70] to develop the corresponding calibration curves.[120] That said, other calculations are possible such as the F/F_0 ratio, where F_0 represents the signal attributed to the control and F is the signal in the presence of the analyte, often ranging from 0 to 1.[15,36] Other authors

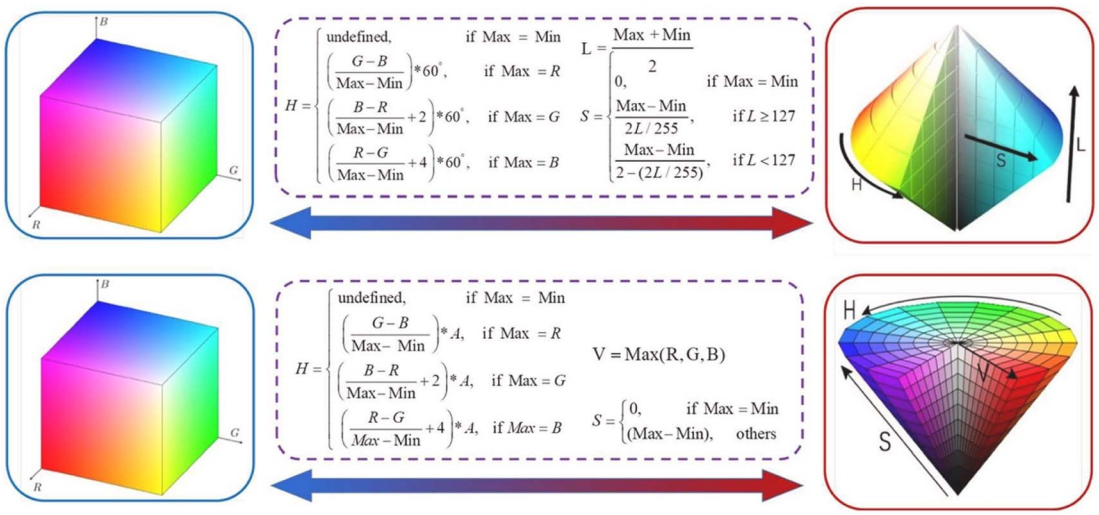

Fig. 2 The conversion relationship between different color spaces. Reprinted with permission from ref. 114.

have also described the possibility of developing these calibration curves using the logarithm of the concentration of the analyte[121] or plotting the concentration as a function of $-\log(F/F_0)$.[60,122] The latter approach is widely used for colorimetric applications.[21,62]

Sometimes, multiple regions of the spectrum need to be considered to capture the color change. In these cases, the signal is calculated using a vectorial representation of all channels (Euclidean distance),[70,85] as shown in eqn (1). Here, the R, G and B values correspond to the image obtained in the presence of the analyte and the R_0, G_0 and B_0 values correspond to the image obtained for the blank.

$$\text{Intensity} = \sqrt{(R-R_0)^2 + (G-G_0)^2 + (B-B_0)^2} \quad (1)$$

Another data processing option is to consider the product of the three RGB channels[76] potentially reaching values as large as 10^7. Both of these options are used for cases when there is a very low variation in RGB values, requiring the use of all the information available[76] and considering that sometimes noise can be introduced in the methodology.[52] Of course, other options to use color values have been described in the literature.[123]

2.3. Apps

To use the data for DI methods, the captured image should be decomposed into the corresponding color values. In this process, different mathematical models are used, as previously commented on. These models are available in different platforms, including Java,[124] Python,[8] and Visual Basic.[125] In this context, applications such as ImageJ,[21,62,98,126] Color Name,[36] Color Grab,[60,122] Dragon RGB,[96] PhotoMetrix,[104,126,127] and ColorX[125] are the most commonly used. Most of these apps are free, and some of them even offer the possibility of using univariate analysis or multivariate partial least squares.[81]

2.4. Analytical validation

As in the case of other analytical methods, validation of DI methods is performed considering the linear range, limits of detection,[128] limits of quantification, selectivity,[129–132] and recovery. While several criteria can be found across the literature, authors are encouraged to adhere to the latest IUPAC recommendations. Here, the LOD can be estimated as: LOD = $2t_{(1-\sigma,\nu)} \times \sigma_0$, where t is the value of Student's tabulated t-test value for ν (degrees of freedom), and σ_0 is the standard deviation of the blank solution. Studies of intra and inter-day repeatability and reproducibility can also be considered to supplement the validation. Additional information related to these parameters can be found elsewhere.[128,133–137]

3. Quantum dots

Quantum dots (QDs) are nanoparticles that present unique and size-dependent properties,[138,139] such as the emission wavelength. Among these, their intense fluorescence and photostability have greatly contributed to their use as analytical probes.[123,140] QDs also feature a rich surface chemistry, which not only allows them to form stable suspensions[123,141] but also opens the door for their conjugation.[138,142–145] QDs can be classified as core, core–shell, or alloy types. Core QDs feature a uniform composition (typically in the form of CdX, X = Se, S or Te),[83,89,142,145] and while they offer excellent quantum yields, their applicability is limited by their toxicity.[123] Core–shell QDs also include a composite shell, normally of type II–VI, IV–VI or III–V semiconductors, such as ZnS, CdS and CdSe. This modification gives them greater photostability and quantum yield.[35,146–150] Alloy-type QDs have the potential to outperform the other configurations because their synthesis process can lead to (at least partially) a more homogeneous electronic structure and to a much wider spectrum of photoluminescence.[151,152] In addition to these, carbon quantum dots (CQDs) have gained considerable attention due to their competitive optical properties,[140] the possibility of being made out of natural substrates,[33,36,48,73,153] their low toxicity, and their surface functionality.[73,74,154,155] CQDs were first described by Ya-Ping Sun[156] and have led, since then, to several generations of hybrid materials (SiO_2-QDs,[157,158] P-QDs,[159,160] S-QDs,[161] and Mn-QDs[162]). Synthesis approaches for the development and modification of QDs are specifically addressed in the literature,[33,138,163] and will only be briefly commented on in this review. Thus, it is then reasonable that many of the advantages of DI have been amplified by the use of QDs, leading to unique sensing approaches[5,162,164] that are clearly gaining interest in the community (Fig. 3).

While this exponential increase is only expected to grow in the next few years, it is important to note that many of the potential advantages of DI-QDs are sometimes limited by long experimental procedures linked to the preparation of the probes, that in many cases still employ toxic reagents and solvents,[165] are not energy efficient (*i.e.* heating at 180 °C for 12 h) and require slow purification steps. Aiming to provide readers an objective account of the advantages and disadvantages of the use of DI-QDs, the following sections provide an

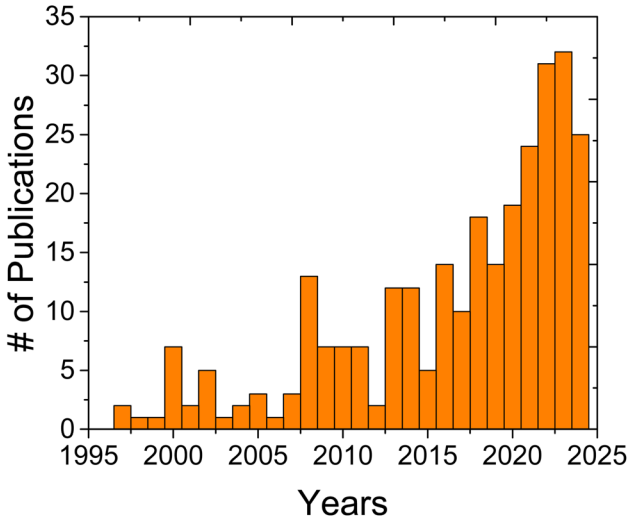

Fig. 3 Trend in publications related to DI-QDs from 1995 to 2024 (November). Data obtained from the Web of Science using digital image and QDs as keywords.

account of representative examples of analytical applications recently reported.

4. Analytical applications of DI-QDs

4.1. DI-QDs for the analysis of food and beverages

One of the most interesting applications of DI-QDs is in the field of food chemistry, as the combination can facilitate the rapid inspection of samples with a user-friendly and familiar interface, thus reducing errors[95,166] and opening the door to more advanced methods based on machine learning.[167] Among other developments, and targeting organophosphorus pesticides (OPs), Tong *et al.*[83] developed a method based on DI-CQDs to analyze strawberries and cherry tomatoes, along with *in situ* extraction. As shown in Fig. 4, the mechanism of this sensor was based on the inhibition of acetylcholinesterase (AChE) by OPs, thus reducing the conversion of acetylthiocholine (ATCh) into thiocholine (TCh), that then coordinates with Ag^+. Thus, the presence of OPs leads to a higher concentration of Ag^+ in the solution, facilitating the oxidation of *o*-phenylenediamine (OPD), and leading to a change in absorbance (at 420 nm) and fluorescence (at 560 nm). The latter causes a quenching effect in the emission of CQDs at 675 nm. The proposed approach featured good selectivity (linked to the use of the enzyme) and a LOD of 0.50 $\mu g L^{-1}$; however, the method also required a relatively long experimental procedure that included several incubation steps and sequential addition of reagents. Moreover, and despite the low sample volume required, the overall analysis time (85 min) may limit its applicability for *in situ* analysis.

Maia *et al.*[36] presented an innovative and cost-effective smartphone FDI method to detect Cu^{2+} in sugar cane spirits. The methodology deployed a UV-LED chamber, a 3D platform crafted from biodegradable polylactic acid (PLA), and a smartphone – that was used for the acquisition of the images. The method was based on the fluorescence quenching of cuprizone-functionalized carbon quantum dots (CPZ-CQDs) derived from rice, prepared *via* a simple hydrothermal route. The authors also employed the Color Name app to analyze sugar cane spirits, leading to a linear range from 2.00 to 7.22 mg L^{-1}, with a limit of detection of 0.23 mg L^{-1}. The range aligns with current limits for Cu^{2+} in distilled beverages set by legislation from Brazil (5 mg L^{-1})[168] or the European Union (2 mg L^{-1}).[169] Moreover, and based on the analysis of variance (ANOVA), the authors concluded that the FDI method was competitive with the traditional method based on atomic absorption spectroscopy (at the 95% confidence level). Although other groups have reported the possibility of quenching fluorescence with copper ions,[44,96,123,170,171] this article was the first application of DI-QDs to the analysis of sugar cane spirits. An innovative smartphone-based platform was also developed for the rapid detection of Cu^{2+} in tea beverages, with the aim of addressing health risks associated with copper accumulation from acidic soils.[96] Here, the authors combined a UV lamp (365 nm) and a sensing reagent (diethyl-[5-(2-1,4,7,10-tetraaza-cyclododec-1-yl-acetylamino)-benzo[α]phenoxazin-9-ylidene]-ammonium, cyclen-NB), leading to a method with good sensitivity (LOD < 5 nmol L^{-1}) and selectivity. Despite these advantages, the synthesis and purification of the probes was considered laborious and involved the use of organic solvents, limiting the greenness of the approach.[12,165] More recently, similar approaches were used to determine iron,[48,172] silver,[173] and pesticides.[18] Along those lines, Patel *et al.*[74] addressed the

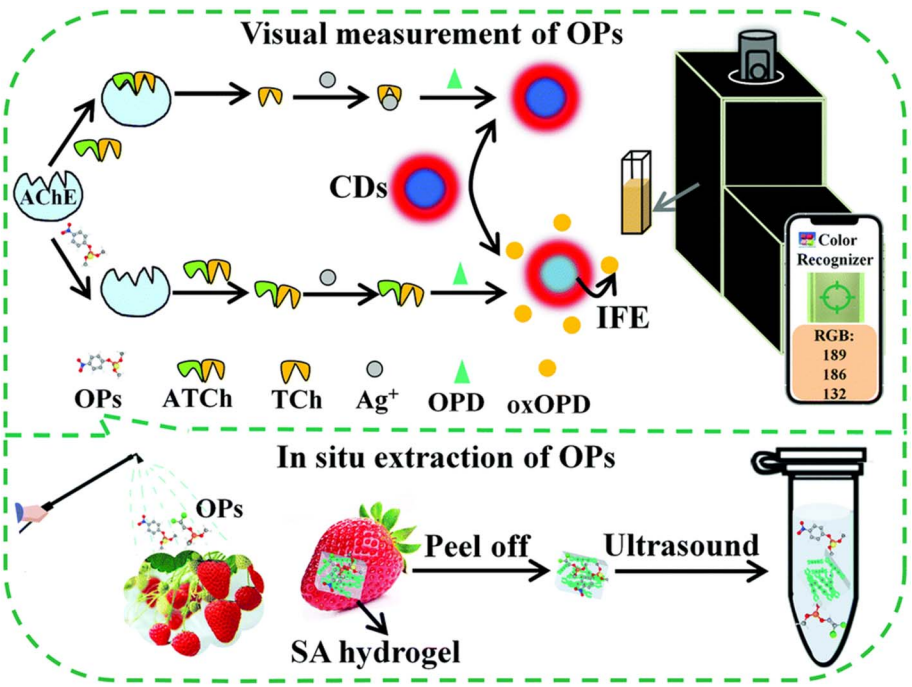

Fig. 4 Schematic illustration of the mechanism for ratiometric fluorescence detection of OPs; smartphone-assisted platform for visually measuring OPs and SA hydrogel for *in situ* extraction of OPs. Reprinted with permission from ref. 83.

increasing use of pesticides in agriculture to improve crop production and pointed out that the residues in water and food had posed health risks. In their work, the authors introduced nitrogen-doped carbon quantum dots (N-CQDs) for the fluorometric detection of methiocarb in vegetables. The method involved a simple, one-step preparation of N-CQDs on paper, utilizing *o*-phenylenediamine for the detection of the pesticide in food. However, the synthesis of N-CQD employed a vacuum oven for 12 h at 180 °C and the DI method employed a conventional UV lamp (instead of a LED or other portable devices with low power consumption). In general, it is important to note that despite their versatility, many of these reports based on optical changes due to the complexation of ions only use spiked samples, do not report MRL units (considered to be more adequate by international agencies[174,175]) and are only partly validated in terms of accuracy.

Another approach to develop DI methods is based on hydrogen bonding or (somewhat) selective interactions between analytes and the QDs. Among these, it is worth mentioning a background-free room temperature phosphorescence (RTP) method for detecting melamine using carbon nitride quantum dots (CN-QDs), embedded in carboxymethyl cellulose (CMC).[31] The CN-QDs-CMC film exhibited a yellow emission, which was quenched in the presence of melamine and captured by a smartphone. The internal hydrogen bonding interactions between CMC and CN-QDs contributed to the confinement effect, suppressing non-radiative relaxation processes, and thus, enhancing quantum yield. This method was validated by testing milk samples from various brands, resulting in recoveries ranging from 92% to 105%, with relative standard deviations (RSD) below 8.6%. A third approach to develop DI-QD sensing approaches is based on the use of enzymes, as selective biorecognition elements. Su *et al.*[30] developed a novel smartphone-based colorimetric method for determining glucose in the presence of glucose oxidase and in various food samples. They also explored the peroxidase-like activity of nitrogen-doped carbon dots (N-CQDs), obtained from locust powder, that facilitated the oxidation of the chromogenic substrate 3,3,5,5-tetramethylbenzidine (TMB) in the presence of H_2O_2, leading to a blue product, with a maximum absorbance at 654 nm. They noted that in the absence of the chromogenic agent, the H_2O_2 can also generate a change in the fluorescence due to its capacity to etch the surface of the carbon dots.[94] The authors compared the results using the DI-CQDs to those obtained using a conventional UV-vis spectrophotometer. According to the authors the calculated *t*-test values were 0.66, 1.08, and 0.77, with all values being lower than the *t*-critical value of 2.78, at the 95% confidence level. In addition to these metrics, it is important to note that a simple sample treatment was used (extraction using 1.0 g of sample and 60 mL of deionized water) and that the authors calculated color intensity using the HSL color system. Quenching can also be accomplished by aggregation, as recently demonstrated for the rapid and highly sensitive detection of alcohol content in beverages.[5] For this application, the authors used a novel three-mode fluorescence-based detection platform using reusable CQDs, leading to a detection limit of 0.12%, and enabling the quantification in eight alcoholic beverage samples (whisky, vodka, tequila, baijiu, white wine, rum, brandy and sake) without any additional sample treatment.

Taking advantage of electrostatic interactions, Hu *et al.*[176] presented a smartphone-based approach that utilized gold nanoparticles and CQDs (Au@CQDs) for the visual and semi-quantitative detection of melamine in milk samples. These non-fluorescent Au@CQDs (due to Förster resonance energy transfer, FRET) were de-aggregated upon the addition of melamine, thus releasing CQDs and increasing the fluorescence. The authors reported a detection limit of 1 μmol L^{-1}, enabling the detection of melamine adulteration in dairy products. Despite its potential advantages, it is worth mentioning that IUPAC recommended[133] an updated calculation for the LOD. Other groups have also used the distance-dependent coupling with neighboring AuNPs for the detection of melamine, with[177] and without smartphones.[138] Li *et al.*[157] introduced a cost-effective, sensitive, and portable detection platform designed for point-of-care analysis of ascorbic acid (AA), to evaluate food quality. They developed a point-of-care sensor composed of a fluorescent paper chip, 3D-printed accessories, and a smartphone, enabling visual and ultrasensitive quantitative detection of AA. The paper chip was manufactured on silicon-doped carbon dots (Si-CQDs), which emitted strong fluorescence signals that were quenched by Fe^{3+} and restored in the presence of AA. This portable detection platform, integrating a fluorescence sensor with a smartphone device, yielded an ultrasensitive method (LOD of 18 nmol L^{-1}) that was validated against HPLC (at the 95% confidence level). However, the Si-CQDs were synthesized using a stainless-steel autoclave at 200 °C for 2 h and then purified by dialysis for 24 h. As mentioned before, these conditions are not aligned with AGREE metrics due to the high energy consumption.[97,165]

Representative examples of the use of DI-QDs reported in the literature for the analysis of food and beverages are summarized in Table 1. Based on these results, it can be concluded that carbon-based QDs are preferred for the development of analytical applications. This trend can be attributed to the low toxicity, photostability, and photoluminescence yield of CQDs,[2,155,156,178,182,183] which can also be easily doped with other elements (such as nitrogen to give N-CQDs) to adjust their properties.[30,74,75] As can also be observed in Table 1, smartphones and RGB were the most commonly used options, probably due to their simplicity and direct correlation with color intensity.

4.2. DI-QDs for biochemical and medical analyses

DI-QD methods have significantly impacted the biochemical and medical fields, as they enable a range of point-of-care solutions. In this context, Park's group[184] proposed a direct detection method for the detection of influenza A (H1N1) virus using QDs, modified with aptamers and using an emission light guide for signal enhancement. As schematically shown in Fig. 5, in the absence of the virus, the energy from the QDs is transferred to a dark quencher conjugated with a guard DNA strand (G-DNA). However, in the presence of the target virus, the G-DNA is released thus restoring the fluorescence signals (ON state). Coupling this approach with a photonic crystal and a low-

Table 1 Representative examples of the use of DI-QDs for the analysis of food and beverages

Chemical sensor	Color system	Software/app	Analyte/compound	Samples	Digital device	Linear range	LOD	Ref.
CQDs	RGB	Color Picker	Ethanol	Beverages	Smartphone	0–100%	0.12%	5
CQDs	HSB	Spotxel Reader	Pyrethroid	Tea/apples/grapes	Smartphone	1–120 μg L^{-1}	6.66 μg L^{-1}	15
Cuprizone-CQDs	RGB	Color Name	Cu^{2+}	Sugar cane spirits	Smartphone	2.00–7.22 mg L^{-1}	0.23 mg L^{-1}	36
N-CQDs	HSL	Color Analyzer	Glucose	Red grape/jujube/rice/maize	Smartphone	5–100 μmol L^{-1}	1.09 μmol L^{-1}	30
N-CQDs	RGB	Color Recognizer	Melamine	Milk	Smartphone	0.18–2.07 mg kg^{-1}	0.06 mg kg^{-1}	31
N-CQDs	RGB	ImageJ	Methiocarb	Vegetables	Smartphone	700–10,000 μg L^{-1}	500 μg L^{-1}	74
CQDs	RGB	Color Picker	Fluoroquinolone	Food and environmental samples	Smartphone	0.85–3.6 μmol L^{-1}	0.26 nmol L^{-1}	75
CQDs	RGB	Color Recognizer	Water	Alcoholic beverage	Smartphone	3–30%	1.2%	118
CQDs	RGB	Color Grab	Carbendazim	Lotus seeds	Smartphone	0–2 μg mL^{-1}	—	148
Si-CQDs	RGB	AA-Tester	Ascorbic acid	Food samples	Smartphone	0–3.0 μmol L^{-1}	18.12 nmol L^{-1}	157
CQDs	RGB	Dragon RGB	Cu^{2+}	Tea/tea beverages	Smartphone	0–200 nmol L^{-1}	4.83 nmol L^{-1}	96
Au@CQDs	HSB	—	Melamine	Milk	Smartphone	1–10 μmol L^{-1}	—	176
CQDs	RGB	Color Grab	Ascorbic acid	Fruits	Smartphone	0.5–16 μmol L^{-1}	0.16 μmol L^{-1}	178
Graphene-QDs	RGB	ImageJ	Phenol (Ph) and polyphenol (Po)	Food, wine and seawater	Smartphone	1.66×10^{-5} to 1.33×10^{-4} mol L^{-1}	4.3×10^{-5} (Ph) and 3.9×10^{-5} mol L^{-1} (Po)	37
CQDs	HSV	Color Scanning	Cr^{6+}, lysine (Ly)	Food	Smartphone	5.3–320 μmol L^{-1} Cr^{6+}, 1 to 75 mmol L^{-1} (Ly)	1.6 μmol L^{-1} Cr^{6+}, 0.3 mmol L^{-1} (Ly)	179
CQDs	RGB, HSV	WeChat	Antibiotic	Milk	Smartphone	0.25–30 μmol L^{-1}	0.079 to 0.514 μmol L^{-1}	180
CQDs	RGB	RGB analysis application	Antibiotic	Food samples	Smartphone	0–100 μmol L^{-1}	99.8 to 176 nmol L^{-1}	181

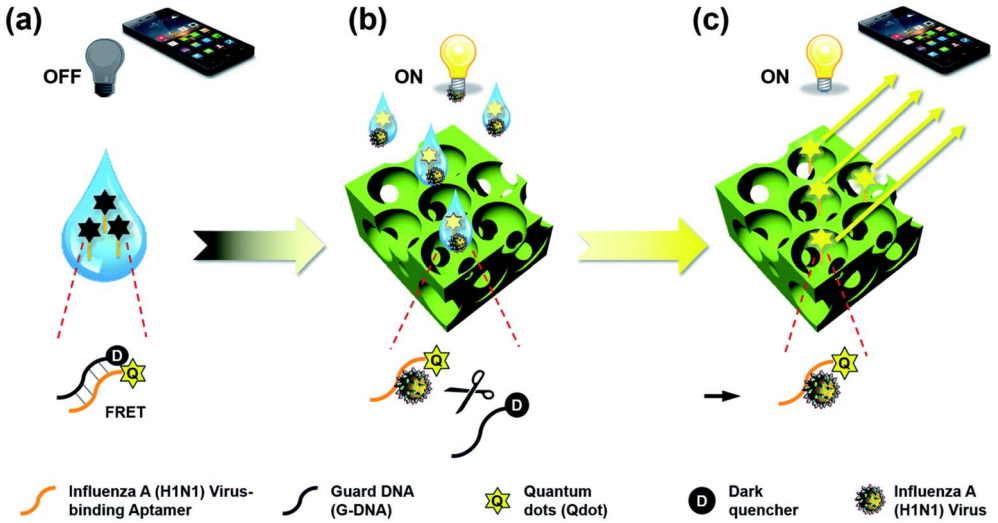

Fig. 5 The proposed "OFF–ON" detection principle using QD-aptamer conjugates and a 3D nanoporous photonic crystal. (a) Loading the prepared quenched QD-aptamer conjugates (*i.e.*, "OFF" state) for influenza A (H1N1) virus detection in aerosol spray. (b) Capturing airborne influenza A (H1N1) virus by aerosol spray and recovering QD signals by releasing G-DNA and preferred aptamer-virus binding (*i.e.*, "ON" state). (c) Visualization of virus detection by the enhanced QD signal owing to the emission light guide in the 3D PC. Reprinted with permission from ref. 184.

end CCD camera allowed them to achieve high sensitivity (LOD = 138 pg mL^{-1}) and high selectivity over other species of influenza A virus (H5N1, H3N2) and biomolecules (thrombin).

Wang *et al.*[164] studied prostate cancer (PrCa), highlighting a critical need for accurate detection of biomarkers in clinical settings to allow early diagnosis and effective treatment. Among those, sarcosine (SAR) has emerged as a promising biomarker for the diagnosis of PrCa, providing viable alternatives beyond the traditional prostate specific antigen (PSA).[185] In this study, a novel ratiometric fluorescence sensor for SAR detection was developed, using Ce(III) as a mediator between 4-methylumbelliferyl phosphate (4-MUP) and CQDs. This sensor takes advantage of the phosphatase-like activity and complexation reaction properties of Ce(IV) to achieve high sensitivity, reaching a detection limit of 89 nmol L^{-1}. The portability and throughput of this approach were further improved by its integration with a simple microfluidic detection platform. Another interesting point of the work includes the absence of toxic reagents. Analytical validation was performed with an interference test with excellent selectivity for SAR in the presence of K^+, Ca^{2+}, Ag^+, Na^+, Fe^{3+}, Cu^{2+}, and some amino acids such as lysine, threonine, histidine, tyrosine, glutamic acid, glycine, and arginine. Moreover, a good linear correlation for SAR concentration was obtained from 0.2 to 150 μmol L^{-1} with recovery values of 95.7–115.0% for detection in urine samples. As previously discussed for food samples,[30,94] Liu *et al.*[186] also described the possibility of using glucose oxidase/H_2O_2 for the fluorescent and colorimetric detection of glucose. Here, a decrease in the emission at 580 nm of CQDs (due to the action of H_2O_2) was followed using a smartphone. More details of this work included a wide linear range of 0.5–450 μmol L^{-1} with a low LOD of 74 nmol L^{-1} for H_2O_2 detection, resulting in an attractive method for analytical applications compared to electrochemistry and spectrofluorometry methods. Moreover, the authors applied statistical tests to certify the precision and accuracy of the method employing spectrofluorometry and UV-Vis spectrophotometry. Additionally, recovery tests rendered results in the ranges of 97.30–102.80% and 95.61–104.58% for fluorescence and colorimetric detection, respectively. The selectivity of the test for glucose was successfully assessed using KCl, $ZnCl_2$, $CuCl_2$, $AlCl_3$, $CdCl_2$, $NiCl_2$, $MgCl_2$, NH_4Cl, $Fe(NO_3)_2$, $Fe(NO_3)_3$, lysine, tryptophan, cysteine, histidine, arginine, glycine, glutathione, hyaluronic acid, sucrose, dopamine, ascorbic acid, fructose and lactose.

Glutathione (GSH) is an antioxidant agent that helps in the detoxification process and disease prevention, so its monitoring in the body where it has a prophylactic function is of fundamental importance. In this context, Chu *et al.*[91] developed a fast and inexpensive method based on CQDs, gold nanoclusters (AuNCs), and copper ions. The mechanism is based on the suppression of fluorescence due to the interaction of nanoparticles with GSH, showing a shift in the fluorescence emission from blue to orange. Using paper and a smartphone integrated into a 3D coupling system, they reported a linear range of 0–50 μmol L^{-1} with a LoD of 1.84 μmol L^{-1}. Moreover, the method presented a good recovery from 97.6 to 105%. Additionally, the probe showed good selectivity to Na^+, K^+, Ca^{2+}, Fe^{2+}, glucose, sucrose, glutamic acid, glycine, arginine, leucine, valine, alanine, threonine, bovine serum albumin, ascorbic acid, cysteine, and homocysteine.

Rong *et al.*[162] developed an important method to detect *Bacillus anthracis* spores, based on the analysis of 2,6-dipicolinic acid (DPA). *Bacillus anthracis* spores have become a particular biothreat concern in recent decades, because their inhalation can lead to death within a few hours. For this method, the authors synthesized functionalized manganese-doped CQDs (Mn-CQDs) through pyrolysis with ethylenediamine, ethylenediamine tetra-acetic acid and Eu(III) ions, leading to a material with an intense blue fluorescence emission at 461 nm. The

Fig. 6 Illustration of the application of DIB and CQDs for monitoring a biocidal agent in a sanitizing mat. Reprinted with permission from ref. 2.

subsequent sensor, based on a shift in fluorescence from blue to red, exhibited a wide linear range (1.0 to 200 μmol L^{-1}), low detection limit (1.0 μmol L^{-1}), and acceptable recoveries (84% to 120%). Moreover, from an environmental point of view, the proposed method met the established requirements, as no toxic reagents were used in the synthesis of CQDs, thus making it a green method.[97,165] Similar CQDs were also synthesized using citric acid and ethylenediamine as precursors and then used for the detection of hypochlorite (Fig. 6)[2] *via* the oxidation of surface-bound furfurals.[68] Here, the intense blue fluorescence was used to monitor biocidal action (during 3 h) in sanitizing carpets, offering a rapid and cost-effective analytical method to minimize the transmission of pathogens.

Ortiz-Gómez *et al.*[158] presented a simple, rapid, and cost-effective approach for producing fluorescent silicon nanodots (SNDs) within a paper-based microfluidic analytical device (μPAD), integrated into a reusable and portable device for total carbohydrate assessment. The synthesis of SNDs employed a redox reaction between (3-aminopropyl) triethoxysilane (APTS) and carbohydrates, the latter acting as reducing agents. To facilitate the synthesis of SNDs, a graphene-based heater was fabricated *via* laser ablation of Kapton polyimide. This configuration required heating of the μPAD at 80 °C for 30 min, promoting the formation of blue-emitting SNDs with a peak emission wavelength at 475 nm. The quantitative analysis of total carbohydrates, expressed as either glucose or fructose index, presented a low detection limit (0.80 μmol per L for glucose and 0.51 μmol per L for fructose). The effectiveness of the proposed method was then demonstrated by determining glucose levels in biological fluids (serum and urine samples) as well as quantifying total carbohydrates in juices and commercial teas. Moreover, the authors described the development of a chamber using an electronic device that allowed the temperature of the μPAD to be controlled during the analysis. Bandi *et al.*[187] synthesized Fe-doped carbon dots (Fe-CQDs) immobilized on cellulose nanofibrils (CNF) *via* a rapid microwave-assisted approach, leading to a substrate with high peroxidase-like activity (POD). The utility of this nanopaper was demonstrated through the oxidation of 3,3′,5,5′-tetramethylbenzidine (TMB) and applied for detection of hydrogen peroxide (H_2O_2) and glucose. Besides the great stability of the substrate (which was stable for a month), one important aspect of this work is that the authors used several color systems (RGB, CMYK, grayscale and CIELAB[116]) for quantification by using the PhotoMetrix PRO app. Concerning the detection of H_2O_2, a linear range of 6–42 μmol L^{-1} and a detection limit of 0.93 μmol L^{-1} were achieved. On the other hand, a linear range of 10–70 μmol L^{-1} with a detection limit of 1.73 μmol L^{-1} was obtained for glucose detection. The method utilized low-cost resources and eco-friendly reagents, such as $FeCl_2 \cdot 4H_2O$, along with biodegradable cellulose nanofibers serving as the test platform. The detection times for H_2O_2 and glucose were 20 minutes and 15 minutes, respectively. Selectivity tests demonstrated that the probe exhibited high specificity for glucose, even in the presence of other carbohydrates like fructose, maltose, lactose, and sucrose. Ren *et al.*[188] introduced an aptamer-based paper sensor adapted for rapid, sensitive, portable and selective detection of the Gram-negative bacterium *Vibrio parahaemolyticus* that is found in coastal areas, and can infect seafood. The approach involved the synthesis of capture probes through the conjugation of CQDs with amino-modified single-stranded DNA. This conjugation acts as a "switch" through hybridization of the aptamer *anti-Vibrio parahaemolyticus* and AuNPs, resulting in the formation of double-stranded DNA structures. Upon exposure to *Vibrio parahaemolyticus*, aptamers within the double-stranded DNA selectively bind to the target bacteria and release the AuNP probes to interact with the capture probes. The fluorescence emitted by CQDs is then greatly affected, transitioning from bright blue to colorless. As is well known, the use of aptamers enables high selectivity,[46] which was demonstrated in the detection of *Vibrio parahaemolyticus* in the presence of other bacteria such as *L. monocytogenes*, *P. aeruginosa*, *S. typhimurium*, *S. aureus*, *E. coli*, and *E. sakazakii*. The analytical curve presented acceptable elements such as low standard deviation, $R^2 = 0.98$ and a good sensitivity for *V. parahaemolyticus*.

Given the key role of alkaline phosphatase (ALP) in the clinical diagnosis of various diseases and physiological research, Wang *et al.*[6] developed a reliable measurement assay with high efficiency and precision. This research employed a readily available solvothermal method to synthesize bifunctional CQDs featuring peroxidase-like and fluorescent properties. While other groups have described similar properties,[30,187,189] a multi-signal detection system was herein reported. This highly sensitive multi-signal detection approach led to a linear range from 0.05 to 1.8 U L^{-1}, and a limit of

Table 2 Representative examples of the use of DI-QDs for biochemical and medical analyses

Chemical sensor	Color system	Software/app	Analyte/compound	Samples	Digital device	Linear range	LOD	Ref.
CQDs	RGB	ImageJ	Hypochlorite	Sanitizing mat	Smartphone	17–90 μmol L^{-1}	3.30 μmol L^{-1}	2
CQDs	RGB	Color Picker	Ethanol	Alcoholic beverage	Smartphone	—	0.19 and 0.16%	5
CQDs	RGB	Color Collection	1,4-Phenylenediamine	Human serum	Smartphone	0.05–1.8 U L^{-1}	0.034 to 0.027 U L^{-1}	6
CQDs	RGB	Analysis Gel Array	Dopamine	Plasma	Smartphone	0.1–1000 μmol L^{-1}	163 μmol L^{-1}	7
N, S-CQDs	RGB	Color Recognizer	Tetracycline	Water	Smartphone	0.08–45 μmol L^{-1}	12 nmol L^{-1}	190
CQDs	RGB and HSV	Artificial Intelligent Assay	Fluoride ion	Food	Smartphone	150–1200 μmol L^{-1}	8 μmol L^{-1}	23
CQDs	RGB	Color Recognizer APP	Glutathione	Human serum	Smartphone, digital camera	0–50 μmol L^{-1}	0.18 μmol L^{-1}	91
CQDs	RGB	Color Picker	4-Nitrophenol	Water	Smartphone	0.110–60 μmol L^{-1}	0.110 μmol L^{-1}	153
SNDs	Gray scale		Glucose (Glu) and Fructose (Fru)	Urine and serum samples	Smartphone	10–200 μmol L^{-1} (Glu), 10–100 μmol L^{-1}(Fru)	0.80 μmol L^{-1} (Glu), 0.51 μmol L^{-1}(Fru)	158
CQDs	RGB	ColorGrab	Sarcosine	Urine	Smartphone	0.2–120 μmol L^{-1}	89 nmol L^{-1}	164
CQDs	RGB	Color Grab	Ascorbic acid	Fruits	Smartphone	0.5–20 μmol L^{-1}	0.16–0.19 μmol L^{-1}	178
Au@-CQDs	RGB	—	*Vibrio parahaemolyticus*	Water	Smartphone	10^2–10^6 CFU mL^{-1}	6.7×10^1 CFU mL^{-1}	188
CQDs	RGB	Camera Color Picker	Thiamethoxam	Pesticide residue	Smartphone	0.125–20 μmol L^{-1}	70.1 nmol L^{-1}	40
CQDs	RGB	Color Picker	Borax	Food	Smartphone	0–400 μmol L^{-1}	0.92 μmol L^{-1}	191
CQDs	RGB	Swatches App	α-Glucosidase	Mouse serum	Smartphone	0.01–0.04 U mL^{-1}	0.001 U mL^{-1}	192
Sulfur–boron-CQDs	RGB	RGB Color Picker	Fe^{3+} and cysteine (Cys)	Cell	Smartphone	0–20 μmol L^{-1} (Fe^{3+}), 0–50 μmol L^{-1}(Cys)	54.4 nmol L^{-1} (Fe^{3+}), 4.9 nmol L^{-1}(Cys)	49

detection of 0.027 U L^{-1}. To facilitate on-site visual detection of ALP, a simple and portable hydrogel-based kit was also assembled, allowing seamless integration with a smartphone for analysis. The selectivity test demonstrated satisfactory performance for ALP in the presence of lysozyme, adenosine deaminase, trypsin, protein kinase A, α-glycosidase, glutathione-*S*-transferase, tyrosinase, thrombin, and amylase.

Complementing these reports, Table 2 presents additional examples of the use of DI-QDs reported in the literature for biochemical and medical analyses.

4.3. DI-QDs for the analysis of drugs

Several analytical methods based on DI-QDs have been recently reported to determine drugs and medicinal products for both human and veterinary uses. In this context, Kujur *et al.*[193] developed N-CQDs using *o*-phenylenediamine (*o*-PD) and urea as precursors, rendering highly fluorescent probes with an emission at 520 nm (Fig. 7). These N-CQDs presented a large quenching effect in the presence of MnO_2-NTs. On the other hand, when glutathione (GSH) and captopril (CAP) were present, the fluorescence of N-CQDs was recovered. The change in the fluorescence of the N-CQDs was measured using a smartphone, and then analyzed converting the image to gray scale color using ImageJ. The proposed method featured limits of detection of 5.76 μmol L^{-1} for glutathione and 2.81 μmol L^{-1} for captopril, enabling accurate measurements of these analytes in human samples.

Han *et al.*[123] also targeted CAP, but using a combination of CQDs and gold nanoclusters (AuNCs). For this purpose, Cu^{2+} ions were added to this probe to interact with the amino and carboxyl groups on the surface of AuNCs, favoring the quenching effect of AuNCs. For this sensing approach, a detection platform combining fluorescent test strips and a smartphone was used, leading to a linear range of 0.25–50 μmol L^{-1}, a LOD of 101 nmol L^{-1}, and recoveries of 92.0–108.0% for assessing urine samples. Moreover, an interference test was performed with threonine, L-valine, L-leucine, phenylalanine, alanine, isoleucine, Na^+, K^+, Ca^{2+}, urea, glucose, CH_3COO^-, Cl^-, NO_3^-, SO_4^{2-}, and glycine.

Castro *et al.*[194] presented a novel sensing platform for the detection of ibandronic acid (IBAN), a bisphosphonate used to treat and prevent osteoporosis, bone fractures, and hypercalcemia. The approach was based on the quenching and signal recovery (in the presence of IBAN) of a combination of CQDs and thiomalic acid (TMA)-capped $AgInS_2$ quantum dots ($AgInS_2$-QDs). Additionally, a visual sensing approach was proposed, utilizing RGB images captured by a digital camera and enabling rapid screening of IBAN.

Meng *et al.*[195] developed a new label-free ratiometric fluorescent sensing method using CQDs for detecting sertraline (SER) and glutathione (GSH). The orange CQDs were synthesized through a simple hydrothermal process using neutral red and polyethyleneimine, displaying potential for intracellular detection of the selected analytes. The method presented a linear range of 5–50 μmol L^{-1} (SER) and 10–110 μmol L^{-1} (GSH) with detection limits of only 3 μmol L^{-1} and 7 μmol L^{-1}, respectively.

Due to the therapeutic importance of antibiotics, which includes the increasing risk of developing bacterial resistance when they are not properly used,[196] several groups have focused their attention on quantifying these drugs in several settings. For instance, Lu *et al.*[180] quantified tetracyclines through a trichromatic probe based on CQDs and copper nanoagglomerates coated with bovine serum albumin (BSA-Cu-

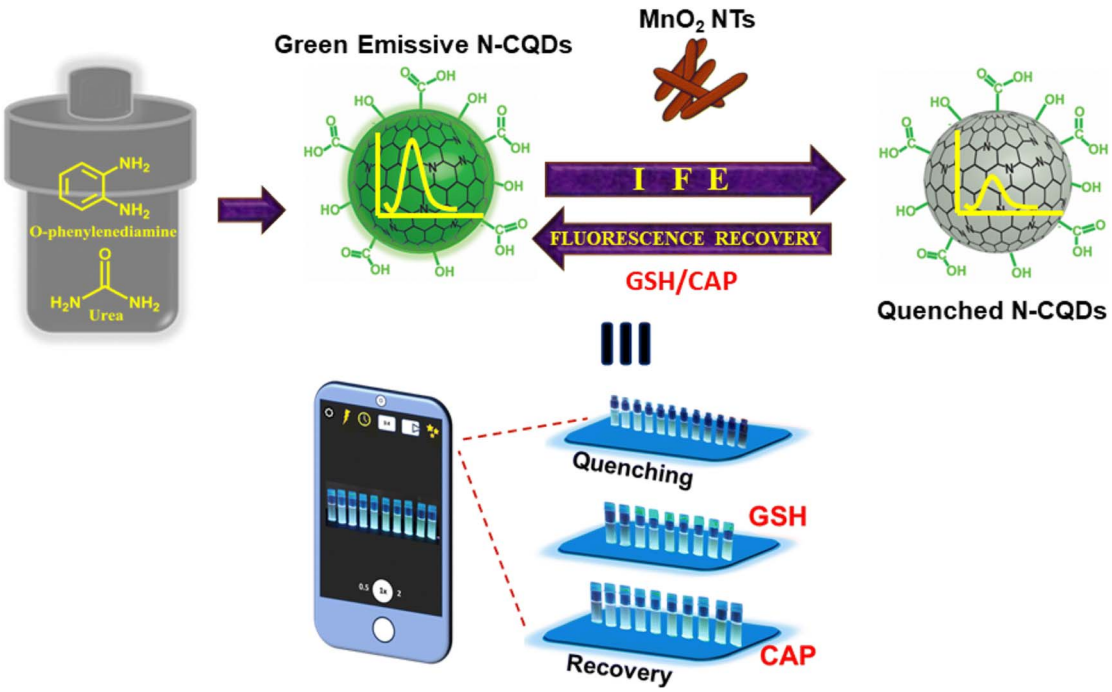

Fig. 7 Schematic representation of the detection of glutathione and captopril. Reprinted with permission from ref. 193.

NCDs, emission at 635 nm). The approach displayed LODs in the range of 0.079 to 0.514 μmol L^{-1} when deployed for tetracycline (TC), oxytetracycline (OTC), chlortetracycline hydrochloride (CTC), and doxycycline (DC). It is important to note that the preparation of BSA-Cu-NCDs involved several experimental steps, including the purification of the NCDs (dialyzed in ultrapure water for 4 days). Also aiming to quantify TC, Cui *et al.*[190] developed a miniaturized device containing a fluorescence test strip, a sample slot, a UV lamp (390 nm), and a smartphone. The authors claim that the addition of Eu^{3+} caused a decrease in fluorescence (at 530 nm) of the selected nitrogen and sulfur co-doped carbon dots (N,S-CQDs) due to the inner filter effect (IEF). Addition of TC did not affect the emission of N,S-CQDs but enhanced the emission of Eu^{3+} (at 616 nm) due to the antenna effect between Eu^{3+} and TC, thus providing the signal for the ratiometric sensor. TC detection was evaluated at three concentration levels, with good recovery (95.55–109.35%) and selectivity towards other antibiotics and metal ions. Similarly, Wu *et al.*[183] developed a selective and sensitive method based on N-CQDs to detect OTC. Here, the interaction between N-CQDs and Eu^{3+} was also used, enabling the use of the ratio between the signal of the N-CQDs (at 445 nm) and that of Eu^{3+} (at 621 nm). In this case, the method was applied to detect OTC in pig muscle and urine, demonstrating great potential for real-time sensing applications. The probe showed good selectivity with respect to K^+, Mg^{2+}, Ca^{2+}, Na^+, Cl^- and CO_3^{2-} and other antibiotics such as florfenicol, penicillin, streptomycin, ampicillin, sulfadiazine, azithromycin, enrofloxacin, and cephalexin. Along the same lines, Zhang *et al.*[41] proposed a portable, rapid, sensitive, and selective method for detecting chlortetracycline (CTC) residues in milk as they pose a potential health hazard for consumers. They successfully prepared a novel fluorescence probe based on nitrogen and phosphorus doped on CQDs and iron-MOF as a molecularly imprinted polymer (N,P-CQDs@MIP). This probe was able to detect the CTC residues by the well-known IFE mechanism. The selectivity of this method was assessed in the presence of oxytetracycline, doxycycline, and tetracycline, which did not induce significant interference. The authors reported that the probe exhibited a strong linear relationship with CTC concentrations ranging from 0.1 to 30 μg mL^{-1}, with a LOD of 0.033 μg mL^{-1}, and recovery rates between 89% and 96%. Wang *et al.*[197] introduced an innovative fluorometric analysis platform utilizing multicolor emissive CQDs. This platform enabled rapid quantification and discrimination of nitroimidazole antibiotic residues, enabling their precise and accurate analysis for food safety evaluation. Here, the fluorescence of the reported CQDs was quenched due to the inner filter effect (IFE) with MNZ. The platform demonstrated satisfactory performance for MNZ detection in real food samples, with a linear range up to 100 μmol L^{-1} and a LOD of 0.45 μmol L^{-1}. The authors performed a recovery test with values ranging from 84 to 106% for DI which was comparable to those of HPLC (91–100%). Jiang *et al.*[123] proposed a novel multiplex chromatic response-based fluorescence detection platform for ultrafast and sensitive detection of norfloxacin (NFX), a quinolone antibacterial agent used to treat skin infections. To detect NFX, terbium ions (Tb^{3+}) were chelated on the surface of CdTe, leading to a sequential fluorescence shift from red to yellow. Furthermore, the ratiometric fluorescent probe was coupled with a smartphone for quantitative detection of NFX using the G/R (green/red) ratio, displaying a linear range of 1–12 μmol L^{-1}, a LOD of 6.03 nmol L^{-1}, and a repose time of only 2 s. A colorimetric sensing platform for monitoring ampicillin (AMP) residues, crucial for combating bacterial resistance, was developed by Lu *et al.*[189] The proposed molybdenum-doped carbon dots (Mo-CQDs) featured peroxidase-like activity and enabled the quantification of AMP in the 0.05 to 100 μg mL^{-1} range, with an estimated LOD of just 12 ng mL^{-1}. Authors reported recovery values for AMP in the 95 to 106% range, which were in agreement with those obtained by the HPLC-UV method. To assess the selectivity of the detection platform, authors tested cysteine, histidine, serine, glucose, ascorbic acid, uric acid, citric acid, and dopamine, with non-significant contributions. As an alternative to the method proposed by Cui,[190] Hemmati *et al.*[198] developed a green method for the synthesis of S,N-CQDs from feijoa leaves. Authors also confirmed, *via* fluorescence lifetime decay spectroscopy, that levodopa (L-DOPA) quenched the fluorescence of the S,N-CQDs *via* a photo-induced electron transfer (PET) mechanism. This innovative method provides a user-friendly approach for L-DOPA detection using smartphones and demonstrates good applicability in complex environments such as human serum and urine samples. Authors reported a LOD of 0.45 μmol L^{-1}, with a linear range of 1–50 μmol L^{-1}, and good selectivity (assessed using L-glutamine, L-cysteine, ascorbic acid, urea, citric acid, NaCl, and $CaCl_2$).

Representative examples of the use of DI-QDs reported in the literature for the analysis of drugs are summarized in Table 3. As expected, a common theme in these reports is the inclusion of specific functionalization steps, conferring selectivity to the QDs and enabling the analysis of more complex samples.

4.4. DI-QDs for the analysis of environmental samples and toxic compounds

As recently noted by Jiang's group, environmental pollutants present in the atmosphere, water bodies, and soil have the potential to spread and affect crops, animals and humans.[39,45] The tremendous diversity in the pollutant's chemical structures, coupled with their toxicity have provided fertile ground for the development of sensing applications based on DI-QDs. This is particularly advantageous given the potential for conducting precise determinations even in remote locations.[14,31,42,143,148,179,197,203,204] Although not considered within the scope of this review, it is important to note that several groups have focused their attention on the potential impact that QDs (especially those made with heavy metals) could have on the environment,[205–207] thus highlighting the importance of alternative materials (such as CQDs). In this context, the detection and quantification of pesticides has been a top priority[39] and the combination of DI-QDs has become a powerful tool for *in situ* analysis.[203,204] Among other developments, Wang *et al.*[208] described the use of N-CQDs (embedded in paper) for the analysis of glyphosine in the 0.25 to 10.0 mmol L^{-1} range in

Table 3 Representative examples of the use of DI-QDs for the analysis of drugs

Chemical sensor	Color system	Software/app	Analyte/compound	Samples	Digital device	Linear range	LOD	Ref.
Eu-CQDs	RGB	Chromaticity pick-up	Tetracycline	Milk, honey and water samples	Smartphone	0.025–20 μmol L^{-1}	8.7 nmol L^{-1}	1
N,S-CQDs	RGB	Color recognizer	Tetracycline	Water samples	Smartphone	0.08–45 μmol L^{-1}	20 nmol L^{-1}	190
N,P-CQD-Fe-MOF	RGB	ColorPicker	Chlortetracycline	Milk	Smartphone	0.1–30 μg mL^{-1}	0.033 μg mL^{-1}	41
Eu-CQDs	RGB	ColorMeter RGB picker	Tetracycline	Water samples	Smartphone	0–3 μg mL^{-1}	—	199
Au@-CQDs	RGB	WeChat	Captopril	Urine	Smartphone	0.25–50 μmol L^{-1}	0.10 μmol L^{-1}	123
Mo-QCDs	RGB	Color Identification	Ampicillin	Water samples	Smartphone	0.05 to 100 μg mL^{-1}	12 ng mL^{-1}	189
$AgInS_2$-CQDs	RGB	Matlab	Ibandronic acid	Pharmaceutical samples	Digital camera	3.1 to 33.2 μmol L^{-1}	3.07 μmol L^{-1}	194
CQDs	RGB	WPS Office	Sertraline (Sr) and glutathione (GSH)	Human serum, urine, sertraline tablets and water	Smartphone	5–45 μ mol L^{-1} (Sr), 10–110 μmol L^{-1} (GSH)	2.76 μmol L^{-1} (Sr), 7.36 μmol L^{-1} (GSH)	195
S,N-CQDs	RGB	Color Detector	Levodopa	Human fluids	Smartphone	1–50 μmol L^{-1}	0.45 μmol L^{-1}	198
CQDs	RGB	Color Grab	Nitroimidazole	Food samples	Smartphone	2–100 μmol L^{-1}	0.45 μmol L^{-1}	197
Eu- CQDs	RGB	World of Color	Tetracycline	Milk	Smartphone	0.1–5 μmol L^{-1}	0.1 μmol L^{-1}	200
S,N-CQDs	RGB	ColorAssist	Isoniazid	Human fluids	Smartphone	5–100 μmol L^{-1}	4.0 μmol L^{-1}	201
N-CQDs	RGB	Color-grab	Doxorubicin	Human fluids	Smartphone	0.2–300 μmol L^{-1}	0.70 μmol L^{-1}	202

flour and fruit juice (Fig. 8). The synthesis of N-CQDs was performed using tea husk powder and melamine (190 °C for 6 h), without involving hazardous materials. Similarly, Patle *et al.*[74] also used N-CQDs embedded in paper to determine methiocarb in vegetables. Another aspect common to these reports is that the N-CQDs were developed by hydrothermal synthesis, using either husk powder and melamine or *o*-phenylenediamine. The method presented a limit of detection (LOD) of 500 μg L^{-1} for measuring methiocarb in vegetables, with a linear range from 700 to 10 000 μg L^{-1} and a calculated LOQ of 1650 μg L^{-1}. Recovery tests showed similar results compared to the reference method (spectrofluorometry). Other groups have also used natural and/or low-cost precursors to render N-CQDs,[48,153,183,198,202] thus providing ample versatility to the process.

Wei *et al.*[203] developed a portable laboratory device in a syringe, integrated with a smartphone detection platform, for rapid detection of glyphosate, one of the most common organophosphorus pesticides (OPs) of agrochemical companies.[209] The method employed gold nanoparticles and ratiometric probes based on SiO_2-CQDs, relying on the inhibition of acetylcholinesterase activity by OPs, which induced color and fluorescence changes. The method allowed precise quantitative analysis of OPs, with a linear range of 0–10 μg L^{-1} and a detection limit of 2.81 nmol L^{-1} for the herbicide. However, the proposed approach presented several analytical steps, including an incubation time of 40 min at 37 °C, followed by an additional 30 min for the reaction to complete. Additionally, a toxic reagent (dichloromethane) was used for the analysis of real samples, hindering the green aspect of the methodology. When compared to a reference UHPLC-MS/MS method, the proposed assay presented minor variations although no statistical analyses were described.[130,137] Yu *et al.*[39] addressed the determination of methyl thiophanate (TM), a widely used fungicide for fruits and vegetables. The detection proposed by the authors was carried out using a dual-emission fluorescent probe. That was achieved by coordinating copper metal–organic framework (Cu-MOF) structures with CQDs, yielding a change in color from blue to pink in the presence of TM. They reported a linear range of 0.031–0.769 μmol L^{-1}, with a LOD of 3.67 nmol L^{-1}, and the possibility of applying it to apple, pear, and tomato samples. Although the method offered great selectivity, the total analysis time (from sample preparation to result) required almost 1 h. Although the fungicide carbendazim (CBZ, commonly used in Brazil and China for agricultural purposes[210]) is banned in the US, the detection of this relevant fungicide was demonstrated by using CQDs and smartphone-integrated paper sensors.[148] The sensing mechanism was based on the red fluorescence quenching induced by CBZ through π–π interactions and a photoinduced electron-transfer effect, leading to a selective and sensitive detection of CBZ within 3 min. Just like other compounds in this group, insecticides have great potential to contaminate soil, groundwater, and surface water.[211] In line with this, Zhu *et al.* presented a novel smartphone-integrated optosensing platform based on red-emission CQDs for the detection of pyrethroids.[15] The synthesis of CQDs was carried out in a straightforward manner, using relatively safe reagents. One drawback of the described method is that it involves considerable sample preparation (heating, centrifugation, filtration, evaporation, and resuspension), posing significant challenges for their use for *in situ* applications.[8,14,27,28,46,81,104] It is also worth mentioning that the platform integrated a portable UV light box combined with a smartphone, leading to a LOD of 7 μg L^{-1} of lambda-cyhalothrin. This work was later extended to include blue-green dual-emission core–shell CQDs rendering a ratiometric sensing platform with a LOD of 0.61 μg L^{-1}, which could meet the needs of real analytical samples.[145]

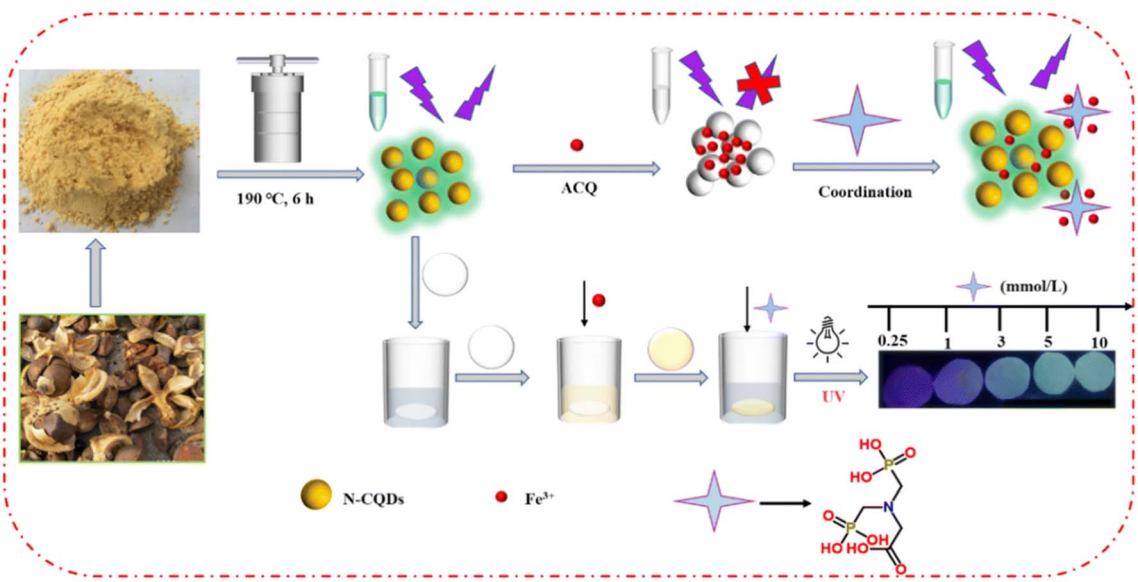

Fig. 8 The illustration of the fluorescent probe based on N-CQDs/Fe^{3+} for the detection of glyphosine. Here, the signal was quenched by Fe^{3+} and then recovered upon the addition of glyphosine. Reprinted with permission from ref. 208.

Table 4 Representative examples of the use of DI-QDs reported in the literature for the analysis of environmental samples and toxic compounds

Chemical sensor	Color system	Software/app	Analyte/compound	Samples	Digital device	Linear range	LOD	Ref.
N-CQDs	RGB	Color Recognizer	Melamine	Aqueous solution	Smartphone	0.18–2.07 mg kg^{-1}	0.06 mg kg^{-1}	31
CQDs	RGB	—	Hg^{2+}, Pb^{2+} and Cu^{2+}	River water	Smartphone	0.12–320 nmol L^{-1}	0.076 to 5.8 nmol L^{-1}	32
CQDs	RGB	Color Name	Hg^{2+}	Water	Smartphone	0.5–45.0 μmol L^{-1}	0.23 μmol L^{-1}	33
CQDs	RGB	Fluorimeter App	H_3O^+	Water/vinegar/soft drink	Smartphone	2.00–12.0 mmol L^{-1}	—	72
N-CQDs	RGB	Color Desk	Ag^+	Water	Smartphone	0–20 μmol L^{-1}	83 nmol L^{-1}	73
CdTe QDs	RGB	WeChat	Tetrachloro-*p*-benzoquinone	River water	Smartphone	0–8 μmol L^{-1}	93 nmol L^{-1}	109
CQDs	RGB, gray scale	Real-time color picker, Xi'an Oupao	Red allura, bright blue, sunset yellow	Waste water	Smartphone	0.1–50 μg mL^{-1}	0.12 to 2.7 μg mL^{-1}	117
CQDs	RGB	Spotxel Reader	Pyrethroids	Tap water, apple and cucumber	Smartphone	1–150 μg L^{-1}	0.048 μg L^{-1}	83
N-CQDs	RGB	RGB APP	4-Nitrophenol	Water	Smartphone	0.083–80 μmol L^{-1}	83 nmol L^{-1}	147
CdTe/ZnS/CdS QDs	RGB	APP	Cd^{2+}	Tap water	Smartphone	1–2000 μg L^{-1}	0.057 μg L^{-1}	150
CQDs	RGB	RGB Analysis	4-Nitrophenol	Tap, waste and river water	Smartphone	0.054–68 μmol L^{-1}	54 nmol L^{-1}	153
N-CQDs	RGB	ImageJ	Cu^{2+}	Water	Smartphone	1–200 nmol L^{-1}	0.43 nmol L^{-1}	155
Graphene-QDs	—	—	Pb^{2+}	Aqueous solution	Smartphone	0.5–40 nmol L^{-1}	0.25 nmol L^{-1}	163
CQDs	RGB	ImageJ and Matlab	2,4-D	Lake water, pear juice, human urine and serum	Smartphone	0–15 mg L^{-1}	100 μg L^{-1}	187
CQDs	RGB	Camera Color Picker	Thiamethoxam	Pesticide residues	Smartphone	0.1–20 μmol L^{-1}	13.5 nmol L^{-1}	40
CQD-Cu-MOF	RGB	Color Analyzer	Thiophanate-methyl	Apple, pear, and tomato	Smartphone	0.0307–0.769 μmol L^{-1}	3.67 nmol L^{-1}	39
SiO_2-CQDs	RGB	Color Detector	Glyphosate	Food	Smartphone	0–10 μgL^{-1}	2.81 nmol L^{-1}	203
CQDs	RGB	ImageJ	Al^{3+}	Tap and lagoon water	Smartphone	15.39–153.85 μmol L^{-1}	5.55 μmol L^{-1}	204
Polymer-CQDs	RGB	Go Spectro	Cypermethrin acid (CyA) and 3-phenoxybenzoic acid (3-PBA)	Aqueous solution	Smartphone	1–100 ng mL^{-1} (CyA), 0.1–100 ng mL^{-1} (3-PBA)	0.35 ng mL^{-1} (CyA), 0.04 ng mL^{-1} (3-PBA)	213
Graphene-QDs	RGB	ImageJ	*o*-Nitrophenol (*o*-NP), *p*-nitrophenol (*p*-NP)	River, rain and tap water	Smartphone	0.3–60 μg mL^{-1} (*o*-NP), 0.2–40 μg mL^{-1} (*p*-NP)	0.07 μg mL^{-1} (*o*-NP), 0.03 μg mL^{-1} (*p*-NP)	214
S-QDs	RGB	Color Detector	Co^{2+}	Aqueous solution	Smartphone	0–200 μmol L^{-1}	—	215
SiO_2-QDs	RGB	ImageJ	Chlorpyrifos	Water	Smartphone	0–100 μg L^{-1}	0.054 mmol L^{-1}	216
Graphene-QDs	RGB	Color Grab	Fe^{3+}	Human serum	Smartphone	0–0.8 mmol L^{-1}	0.05 mmol L^{-1}	217
CdTe QDs	RGB	WeChat	Ag^+	River water	Smartphone	0.125–12.5 μmol L^{-1}	40 nmol L^{-1}	218
SiO_2-QDs	RGB	Color Picker	F^-	Water	Smartphone	0–70.0 μmol L^{-1}	2.0 μmol L^{-1}	219
CdTe QDs	RGB	—	Hg^{2+}	Tap water	Smartphone	5–300 nmol L^{-1}	1 nmol L^{-1}	220
CdTe QDs	RGB	—	Formaldehyde	Air	Smartphone	0–1 mg L^{-1}	0.08 mg L^{-1}	221
CQDs	RGB	ImageJ	Chlorine	Water	Smartphone	20–500 μg L^{-1}	6 μg L^{-1}	222
N-CQDs	RGB	ImageJ	Cr^{6+}	Water, soil	Smartphone	0.2–150 μmol L^{-1}	0.058 μmol L^{-1}	223
CdTe QDs	RGB	RGB test	Norfloxacin	Lake water	Smartphone	1–12 μmol L^{-1}	6.03 nmol L^{-1}	224
Si-QDs	RGB	ImageJ	Paraoxon	Food	Smartphone	10–500 ng mL^{-1}	10 ng mL^{-1}	225

The quantification of various inorganic ions is also of paramount environmental importance and several of them have been addressed by DI-QDs. Among those, Maia *et al.*[33] developed a method for quantifying Hg^{2+} in water, using a simple and inexpensive process to synthesize CQDs through rice starch hydrolysis. The synthesis employs a simple, low-cost, and environmentally friendly methodology due to use of 20 g of rice with 20 mL of deionized water. Leveraging biomass from banana petioles, Korram *et al.*[48] synthesized N-CQDs for selective analysis of the micronutrient Fe^{3+}, achieving a LOD of 0.21 nmol L^{-1}. This was accomplished using a switch-off mechanism involving the formation of a non-radiative charge transfer complex through a photoinduced electron transfer process, similar to the mechanism reported by Hemmati *et al.*[198] The synthesis was performed by using environmentally friendly reagents, starting from banana petioles and water (hydrothermal reactor, 5 h at 200 °C). Aiming to determine nitrite levels in soil and water (crucial for monitoring environmental ecosystems and agricultural productivity), Das *et al.*[212] presented a new detection approach based on CQDs modified with neutral red (NR). In this system, implemented through a detection platform integrated with a smartphone, the CQDs served as energy donors and NR acted as an energy acceptor. The presence of nitrite in the CQDs-NR led to an increase in fluorescence intensity at 563 nm, after excitation at 375 nm.

Representative examples of the use of DI-QDs reported in the literature for the analysis of environmental samples and toxic compounds are summarized in Table 4.

4.5. DI-QDs for the analysis of forensic samples

Forensic investigations rely on the fast and accurate analysis of the evidence, an aspect that has promoted the use of a wide variety of DI-QDs as they can minimize the chances of error and speed up the assessment of crime scenes. Addressing one of the most common pieces of evidence, DI-QDs have greatly enhanced forensic fingerprint analysis,[82,89,149,226,227] especially by providing highly fluorescent powders to visualize, as expected, fingerprints. For example, Wang *et al.*[182] proposed a method based on CQDs synthesized by microwave radiation, allowing the identification of latent fingerprints with high definition and contrast (Fig. 9). The methodology was aligned with green chemistry principles by utilizing a one-step, straightforward preparation process that minimizes the need for hazardous chemicals.[26,97,165,198] To demonstrate the robustness of the detection method, interference tests were performed using substances that could be reasonably expected in a crime scene such as acetic acid, sodium chloride, and ethyl alcohol.

Similarly, Yuan *et al.*[71] developed an innovative approach towards fingerprint sensing, presenting a comprehensive exploration of the synthesis, mechanism, and application of CQDs (from rhodamine 6G and rhodamine B) incorporated within diatomite composites. This combination not only represented a low-cost and environmentally friendly alternative to detect fingerprint residues but also proved highly effective in eliminating background interferences, particularly on challenging surfaces such as multicolored or patterned substrates. Large quantities of N-CQDs were also synthesized from *o*-phenylenediamine[227] or polyvinylpyrrolidone,[149] bypassing complex purification and drying processes, rendering powders that can be used for rapid visualization of latent fingerprints on diverse surfaces, including porous and non-porous materials. Milenkovic[149] noted that the material can be used as-received and is non-toxic, as opposite to the lead carbonate powder routinely used by the Spanish police. More importantly, the presence of

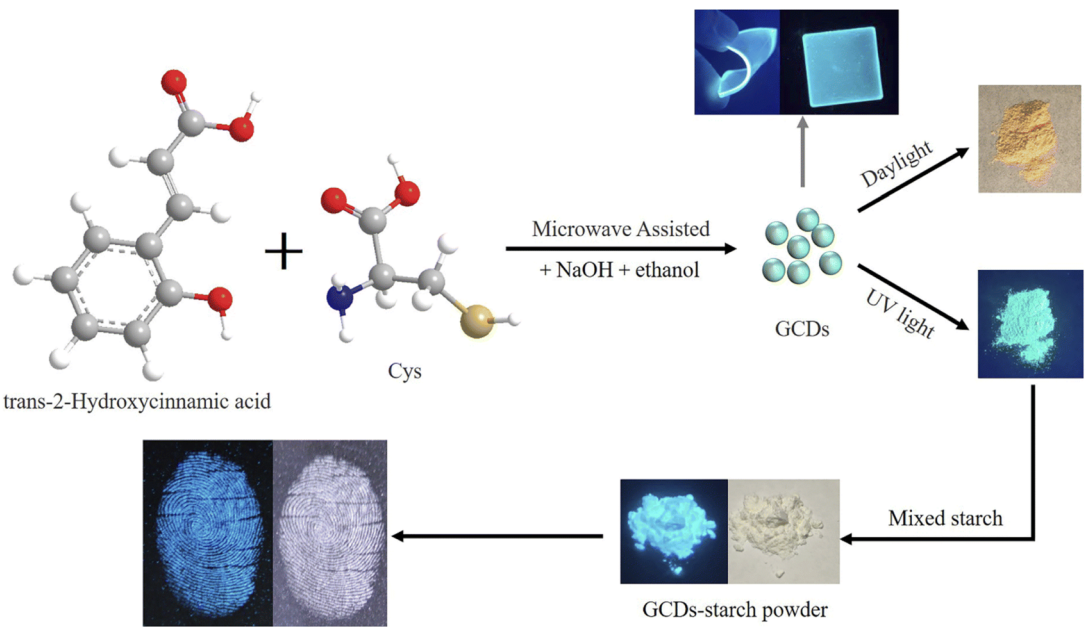

Fig. 9 Research scheme for the one-step facile preparation of carbon dots with high fluorescence quantum yield and application in rapid latent fingerprint detection. Reprinted with permission from ref. 182.

metal ions (Fe^{3+}, Cu^{2+}), organic compounds (fatty acids, amino acids), or compounds present in the matrix of cosmetics showed no significant interference. Zhao *et al.*[228] presented a method for recognizing sweat latent fingerprints using CQDs synthesized from malic acid and ethylenediamine. The experiments demonstrated that optimal fingerprint images were obtained when developing latent fingerprints at pH 9 for 30 min at room temperature, even allowing the identification of water-immersed fingerprints. Although the authors mentioned that the validation of the results was performed, the article does not specify the statistical test employed.[132,136] A bifunctional composite powder consisting of Fe_3O_4@SiO_2-CD was synthesized by Ding *et al.*[89] through a layer-by-layer assembly route, exhibiting both moderate magnetic properties and intense fluorescence. The core–shell structure presented a high fluorescence at 434 nm with a quantum yield of 45% when excited at 370 nm. This nanocomposite powder demonstrated high contrast, sensitivity, and selectivity in enhancing latent fingerprints, surpassing traditional methods.

As noted in a recent review by Alonzo,[229] the analysis of drugs in the field is an important function of law enforcement agencies and forensic drug laboratories. Aiming to improve the selectivity and display differences in the luminescence for each illicit drug measured, Yen *et al.*[230] used CQDs modified with the Marquis reagent. The Marquis reagent is composed of a mixture of formaldehyde and concentrated sulfuric acid used to identify alkaloids and drugs such as methamphetamine, cocaine, heroin and others.[231] The approach, coupled with a deep learning algorithm to find the fluorescence patterns generated by the CQDs, facilitated the fast identification of cocaine and 4-chloroethcathinone. The selectivity of the method was demonstrated for illicit drugs (*e.g.*, methamphetamine and cocaine) in the presence of interferents (*e.g.*, caffeine, paracetamol, and excipients) that could be present in drug mixtures or dilutions. This new methodology can be a viable and efficient alternative at crime scenes, offering significant advantages in terms of cost, portability, and response time; however, the low sensitivity could be a problem when transferring the approach to biological samples.

Homemade explosives[232] and improvised explosive devices (IEDs) represent a permanent challenge for public agencies, especially considering the ever-changing type of explosives employed by criminals.[233] In this category, and aiming to detect low quantities of trinitrotoluene (TNT), Santonocito *et al.*[8] proposed a low-cost method for manufacturing an array-based sensor, containing Bodipy, naphthalimide and CQDs functionalized with different aliphatic chain lengths (CQDs-C_2-OH, CQDs-C_3-OH and CQDs-C_4-OH), providing differential hydrogen bonds and π–π bonds. The results obtained were analyzed by multivariate methods (PLS-DA model) to increase the accuracy aiming to detect not only TNT, but also Amatol, Premex, ANFO (ammonium nitrate fuel oil), dynamite, and PEP (propellants, explosives, and pyrotechnics). The method also showed selectivity for TNT over cyclotrimethylenetrinitramine, pentaerythritol tetranitrate, potassium nitrate, and ammonium nitrate. In addition, Kathiravan *et al.*[226] demonstrated the possibility of detecting picric acid in latent fingerprints using CQDs synthesized from citric acid and thiourea. According to the authors the method was very sensitive (0.1 μmol L^{-1} to 0.5 μmol L^{-1} with a LOD of 12 nmol L^{-1}) and selective (against various nitro compounds such as 2,4-nitrophenol, *p*-nitrophenol, *o*-nitrophenol, *m*-nitrophenol, nitrobenzene, dinitrobenzene, *etc.*). Tawfik *et al.*[234] developed multiple emitting amphiphilic conjugated polythiophene-coated CdTe QDs for the determination of 2,4,6-trinitrophenol (TNP) at picogram levels. For this, cationic polythiophene nanohybrids (CPT-QDs), nonionic polythiophene nanohybrids (NPT-QDs), anionic polythiophene nanohybrids (APT-QDs), and thiophene copolymer nanohybrids (TCP-QDs) were synthesized using an *in situ* polymerization technique. The fluorescence quenching mechanism was based on inner filter effects, electrostatic interactions and hydrogen bonding between the QDs and the explosives. The methodology presented was considered practical and efficient, offering a simple and rapid solution compared to reference methods such as thin-layer chromatography, gas chromatography, and mass spectrometry. Moreover, a low LOD of 0.56 nmol L^{-1} was obtained with a response time of only 60 s.

Table 5 Representative examples of the use of DI-QDs reported in the literature for the analysis of forensic samples

Chemical sensor	Color system	Software/app	Analyte/compound	Samples	Digital device	Linear range	LOD	Ref.
CQDs	RGB	Artificial intelligence-Python	TNT	Explosives	Smartphone	98 ng–985 μg	—	8
Fe_3O_4–SiO_2-CQDs	Grey scale	ImageJ	—	Fingerprint	Digital camera	—	—	89
N-CQDs	RGB	Unscrambler		Tweezers and plastic bag	Digital camera	—	—	149
CQDs	RGB	—	Nitroimidazole antibiotic residues	Fingerprint	Smartphone	—	0.45 μmol L^{-1}	197
CQDs	RGB	—	Picric acid	Fingerprint	Smartphone	0.1–4.0 μmol L^{-1}	0.68 μmol L^{-1}	226
CQDs	RGB	ImageJ	—	Fingerprint	Smartphone	—	—	227
CQDs	RGB	—	Latent fingerprints	Foil paper	Digital camera	—	—	228
CQDs		ColorAssist	Methamphetamine	Drugs	Smartphone	0.1–2.5 mg mL^{-1}	0.02 mg mL^{-1}	230
Paper-CQDs		—	Cocaine, heroin and 4-chloroethcathinone (4-Cec)	Urine	Smartphone	2.000–12.500 ng mL^{-1} for 4-Cec	1.300 ng mL^{-1} for 4-Cec	238

Additionally, the method presented a good recovery from 98.02 to 107.50%.

Chemical warfare agents (CWAs) are highly toxic compounds designed to incapacitate large numbers of soldiers by causing extensive damage to the skin, eyes, and respiratory systems (blisters, swelling, and necrosis) or by binding to acetylcholinesterase and causing respiratory failure.[235] Thus, analytical methods that can accurately detect CWAs are essential to global security measures and for forensic analysis, making fluorescent probes into indispensable tools to this end.[236] Aiming to address the need for efficient, selective, and sensitive sensors to detect CWAs in both water and air environments, Tuccitto *et al.*[237] described the design and synthesis of a fluorescent nanosensor employing CQDs covalently functionalized with ethanolamine. This sensor presented supramolecular interactions with nerve agents, ensuring highly efficient and selective molecular recognition, with a sensitivity of parts per trillion (ppt) in water and sub-ppm levels in air. More details of this method included a supramolecular approach and machine vision to reduce the waste generation mainly for the use of hazardous chemicals compared to reference techniques like gas chromatography-mass spectrometry. A selectivity test was performed to detect trinitrotoluene in the presence of water, CO_2, NO and CO, triethyl-phosphite, phosphocholine, triphenylphosphine and methanol, and no significant interference was obtained. Moreover, the authors reported a low LOD of 10 ng kg^{-1}.

Representative examples of the use of DI-QDs reported in the literature for the analysis of environmental samples and toxic compounds are summarized in Table 5.

5. Conclusions and future prospects

Overall, the combination of DI-QDs represents a powerful option to measure different analytes in diverse matrices with good accuracy and precision. This combination is witnessing an exponential increase despite the relatively small number of publications (<50 per year) specifically addressing this topic. It is notable that smartphones are used in the vast majority of the publications described, due to their growing computing capacity, quality of the cameras included, and number of apps available. In terms of materials, the landscape is clearly dominated by CQDs, probably due to the incredible diversity of precursors available and the simplicity of the hydrothermal process. In general, these CQDs feature a blue emission that can be quenched by a variety of analytes *via* inner filter effects, electrostatic interactions, hydrogen bonding, and redox processes. Although these processes are rather generic, the selectivity of the interaction can be controlled by the addition of ions (copper, iron, silver, *etc.*), polymers, additional materials (AuNPs, MIPs, MOFs, *etc.*), or biorecognition elements (enzymes, aptamers, DNA, *etc.*). The versatility and greenness of the methods are being increasingly reported in the literature, providing a way to compare the environmental impact of the methods reported. The integration of machine learning methods seems to be an emerging trend in the field, not only automating the conversion from signal to concentration but also facilitating the objective interpretation of color changes. Another field that is open for development is the integration of (natural) deep eutectic solvents[24–27] with DI-QDs, providing the opportunity to tune interactions with the analytes and avoiding the use of traditional organic solvents. All things considered, the development of analytical protocols based on DI-QDs is growing and can soon become integrated and connected with other sensors, opening the door to the development of multi-analyte arrays or even networks of sensors.

Data availability

Data reported in this manuscript will be made available upon reasonable request to the corresponding authors.

Author Contributions

João Paulo B. de Almeida: conceptualization, investigation, methodology, project administration, resources, software, validation, visualization, writing – original draft, writing – review & editing. Thomas Tributino: conceptualization, investigation, methodology, project administration, visualization, writing – original draft, writing – review & editing. José R. Sabino: conceptualization, investigation, methodology, visualization, writing – original draft, writing – review & editing. Elias Vinicius: conceptualization, investigation, methodology, visualization, writing – original draft, writing – review & editing. Claudinéia R. S. Oliveira: conceptualization, investigation, methodology, project administration, visualization, writing – original draft, writing – review & editing. Matheus V. Maia: conceptualization, investigation, methodology, project administration, visualization, writing – original draft, writing – review & editing. Willian T Suarez: conceptualization, funding acquisition, investigation, methodology, project administration, resources, software, visualization, writing – original draft, writing – review & editing. Lucas B. Ayres: investigation, software, writing – original draft, writing – review & editing. Carlos D. Garcia: conceptualization, funding acquisition, investigation, methodology, project administration, resources, supervision, visualization, writing – original draft, writing – review & editing. Vagner B. dos Santos: conceptualization, data curation, funding acquisition, investigation, methodology, project administration, resources, software, supervision, validation, visualization, writing – original draft, writing – review & editing.

Conflicts of interest

There are no conflicts to declare.

Acknowledgements

The authors would like to acknowledge the Fundação de Amparo à Ciência e Tecnologia de Pernambuco (FACEPE) (grants APQ-0942-1.06/22 and APQ-0413-1.06/21), the Conselho Nacional de Ciência e Tecnologia (CNPQ) (grants CNPQ 421147/2018-0, 200421/2023-9, and 308422/2023-6) and CAPES for

scholarship. Financial support from the Department of Chemistry at Clemson University is also acknowledged.

References

1 L. Jia, R. Chen, J. Xu, L. Zhang, X. Chen, N. Bi, J. Gou and T. Zhao, *J. Hazard. Mater.*, 2021, **413**, 125296.
2 J. P. B. de Almeida, V. B. dos Santos, G. A. do Nascimento, W. T. Suarez, W. M. de Azevedo, A. F. Ferreira and M. V. Maia, *Anal. Methods*, 2022, **14**, 2631–2641.
3 C. W. Yichao, K. Iris, J. M. Philip, M. Azusa, B. Jiachuan, X. Lizhen, C. Yonghong and S. D. Ralph, *J. Biomed. Opt.*, 2014, **19**, 085002.
4 A. Priye, S. W. Bird, Y. K. Light, C. S. Ball, O. A. Negrete and R. J. Meagher, *Sci. Rep.*, 2017, **7**, 44778.
5 C. Wang, J. Li, X. Wang, Z. Zhao, R. Yao, Y. Jiang, S. Wei, Z. Wang and G. Sun, *Sens. Actuators, B*, 2023, **397**, 134690.
6 S. Wang, B. Han, M. Chen, Y. Han, J. Liu and G. Wang, *Mater. Des.*, 2023, **232**, 112172.
7 G. Chellasamy, S. R. Ankireddy, K.-N. Lee, S. Govindaraju and K. Yun, *Mater. Today Bio*, 2021, **12**, 100168.
8 R. Santonocito, N. Tuccitto, V. Cantaro, A. B. Carbonaro, A. Pappalardo, V. Greco, V. Buccilli, P. Maida, D. Zavattaro, G. Sfuncia, G. Nicotra, G. Maccarrone, A. Gulino, A. Giuffrida and G. Trusso Sfrazzetto, *ACS Omega*, 2022, **7**, 37122–37132.
9 R. S. Lamarca and P. C. F. d. Lima Gomes, *Microchem. J.*, 2020, **152**, 104297.
10 M. Cerrato-Alvarez, S. Frutos-Puerto, P. Arroyo, C. Miró-Rodríguez and E. Pinilla-Gil, *Sens. Actuators, B*, 2021, **338**, 129867.
11 B. Brandoli, G. Spadon, T. Esau, P. Hennessy, A. C. P. L. Carvalho, S. Amer-Yahia and J. F. Rodrigues Jr, *Comput. Electron. Agric.*, 2021, **180**, 105906.
12 L. M. A. de Oliveira, V. B. dos Santos, E. K. N. da Silva, A. S. Lopes and H. A. Dantas-Filho, *Talanta*, 2020, **206**, 120219.
13 F. J. V. Gomez, E. Vidal, C. E. Domini, G. Zanini, M. F. Silva and C. D. Garcia, *J. Mol. Liq.*, 2023, **383**, 122040.
14 J. L. D. Nelis, A. S. Tsagkaris, M. J. Dillon, J. Hajslova and C. T. Elliott, *TrAC, Trends Anal. Chem.*, 2020, **129**, 115934.
15 X. Zhu, X. Yuan, L. Han, H. Liu and B. Sun, *Biosens. Bioelectron.*, 2021, **191**, 113460.
16 S. Soares, K. G. Torres, E. L. Pimentel, P. B. Martelli and F. R. P. Rocha, *Talanta*, 2019, **195**, 229–235.
17 M. d. O. K. Franco, W. T. Suarez, V. B. dos Santos and I. S. Resque, *Food Chem.*, 2021, **338**, 127800.
18 Y. Wang, Y. Ma, H. Wang, F. Shang, B. Yang and Y. Han, *Food Chem.*, 2024, **441**, 138413.
19 J. P. B. de Almeida, V. d. A. Carvalho, L. P. da Silva, M. L. do Nascimento, S. B. de Oliveira, M. V. Maia, W. T. Suarez, C. D. Garcia and V. B. dos Santos, *Anal. Methods*, 2023, **15**, 4827–4833.
20 E. Vidal, C. E. Domini, D. C. Whitehead and C. D. Garcia, *Sens. Diagn.*, 2022, **1**, 496–503.
21 L. P. d. S. Benedetti, V. B. dos Santos, T. A. Silva, E. B. Filho, V. L. Martins and O. Fatibello-Filho, *Anal. Methods*, 2015, **7**, 4138–4144.
22 M. Dupont and J. E. Moore, *Phys. Rev. B*, 2022, **106**, L041109.
23 L. Yan, B. Zhang, Z. Zong, W. Zhou, S. Shuang and L. Shi, *J. Colloid Interface Sci.*, 2023, **651**, 59–67.
24 A. B. Abdullahi, S. Ismail, U. Alshana and N. Ertaş, *J. Food Compos. Anal.*, 2023, **119**, 105263.
25 L. Zhao, Z. Zhang, H. Jiang, Y. Guo, Z. Chen, X. Wang and X. Jing, *Talanta*, 2023, **265**, 124831.
26 A. S. Lorenzetti, E. Vidal, M. F. Silva, C. Domini and F. J. V. Gomez, *ACS Sustainable Chem. Eng.*, 2021, **9**, 5405–5411.
27 V. B. dos Santos, L. B. Ayres, H. Santos, C. D. Garcia and W. Toito Suarez, *Sens. Diagn.*, 2024, **3**, 1467–1475.
28 S. Di Nonno and R. Ulber, *Analyst*, 2021, **146**, 2749–2768.
29 E. Jang and H. Jang, *Chem. Rev.*, 2023, **123**, 4663–4692.
30 K. Su, G. Xiang, C. Cui, X. Jiang, Y. Sun, W. Zhao and L. He, *Arabian J. Chem.*, 2023, **16**, 104538.
31 Y. Kong, T. Lei, Y. He and G. Song, *Food Chem.*, 2022, **390**, 133135.
32 M. Xiao, Z. Liu, N. Xu, L. Jiang, M. Yang and C. Yi, *ACS Sens.*, 2020, **5**, 870–878.
33 M. V. Maia, W. T. Suarez, V. B. dos Santos, S. C. B. de Oliveira and J. P. B. de Almeida, *J. Appl. Chem. Biotechnol.*, 2024, **99**, 1157–1164.
34 V. B. d. Santos, E. F. S. Campos, J. P. B. de Almeida, W. T. Suarez, C. R. S. Oliveira and S. C. B. de Oliveira, *Microchem. J.*, 2023, **189**, 108508.
35 W. Li, X. Zhang, C. Miao, R. Li and Y. Ji, *Anal. Chim. Acta*, 2020, **412**, 2805–2813.
36 M. V. Maia, W. T. Suarez, V. B. dos Santos and J. P. B. de Almeida, *Microchem. J.*, 2022, **179**, 107500.
37 R. Álvarez-Diduk, J. Orozco and A. Merkoçi, *Sci. Rep.*, 2017, **7**, 976.
38 J. L. de Oliveira, W. Toito Suarez, V. B. dos Santos, L. P. da Silva and L. F. Capitán-Vallvey, *Anal. Methods*, 2023, **15**, 5683–5691.
39 Y. Yu, G. Huang, X. Luo, W. Lin, Y. Han, J. Huang and Z. Li, *Microchim. Acta*, 2022, **189**, 325.
40 Y. Dai, W. Xu, J. Hong, Y. Zheng, H. Fan, J. Zhang, J. Fei, W. Zhu and J. Hong, *Biosens. Bioelectron.*, 2023, **238**, 115559.
41 J. Zhang, Y. Liu, X. Cui, Y. Cao, Y. Li, G. Fang and S. Wang, *J. Agric. Food Chem.*, 2023, **71**, 16303–16309.
42 M. Ganesan and P. Nagaraaj, *Anal. Methods*, 2020, **12**, 4254–4275.
43 K. E. McCracken and J.-Y. Yoon, *Anal. Methods*, 2016, **8**, 6591–6601.
44 F. Zu, F. Yan, Z. Bai, J. Xu, Y. Wang, Y. Huang and X. Zhou, *Microchim. Acta*, 2017, **184**, 1899–1914.
45 C. Niu, Z. Yao and S. Jiang, *Sci. Total Environ.*, 2023, **882**, 163565.
46 A. Roda, E. Michelini, M. Zangheri, M. Di Fusco, D. Calabria and P. Simoni, *TrAC, Trends Anal. Chem.*, 2016, **79**, 317–325.
47 A. R. Kirmani, J. M. Luther, M. Abolhasani and A. Amassian, *ACS Energy Lett.*, 2020, **5**, 3069–3100.
48 J. Korram, P. Koyande, S. Mehetre and S. N. Sawant, *ACS Omega*, 2023, **8**, 31410–31418.

49 S. Mohandoss, N. Ahmad, M. Rizwan Khan, K. Sakthi Velu, K. Kalaiselvi, S. Palanisamy, S. You and Y. Rok Lee, *Spectrochim. Acta, Part A*, 2023, **302**, 123040.
50 P. M. Epperson, J. V. Sweedler, R. B. Bilhorn, G. R. Sims and M. B. Denton, *Anal. Chem.*, 1988, **60**, 327A–335A.
51 N. Maleki, A. Safavi and F. Sedaghatpour, *Talanta*, 2004, **64**, 830–835.
52 E. d. N. Gaiao, V. L. Martins, W. d. S. Lyra, L. F. d. Almeida, E. C. d. Silva and M. C. U. Araújo, *Anal. Chim. Acta*, 2006, **570**, 283–290.
53 M. de Oliveira Krambeck Franco, W. T. Suarez and V. B. d. Santos, *Food Anal. Methods*, 2017, **10**, 508–515.
54 K. D. Pessoa, W. T. Suarez, M. F. dos Reis, M. de Oliveira Krambeck Franco, R. P. L. Moreira and V. B. dos Santos, *Spectrochim. Acta, Part A*, 2017, **185**, 310–316.
55 S. Soares, M. J. A. Lima and F. R. P. Rocha, *Microchem. J.*, 2017, **133**, 195–199.
56 J. Caleb, U. Alshana and N. Ertaş, *Food Chem.*, 2021, **336**, 127708.
57 E. Vidal, A. S. Lorenzetti, C. D. Garcia and C. E. Domini, *Anal. Chim. Acta*, 2021, **1151**, 338249.
58 W. T. Suarez, O. D. Pessoa-Neto, V. B. dos Santos, A. R. de Araujo Nogueira, R. C. Faria, O. Fatibello-Filho, M. Puyol and J. Alonso, *Anal. Chim. Acta*, 2010, **398**, 1525–1533.
59 S. Soares and F. R. P. Rocha, *Microchem. J.*, 2021, **162**, 105862.
60 M. de Oliveira Krambeck Franco, W. T. Suarez, G. R. P. Pereira, C. B. Vilanculo, M. C. R. Vieira, V. B. dos Santos and J. P. B. de Almeida, *Microchem. J.*, 2023, **187**, 108416.
61 W. S. Claudinéia Oliveira, H. R. Nahas, F. Junior Moreira Novaes, J. P. Almeida and V. Bezerra dos Santos, *Rev. Virtual Quim.*, 2024, **16**, 307–326.
62 L. Pires dos Santos Benedetti, V. Bezerra dos Santos, T. A. Silva, E. Benedetti-Filho, V. L. Martins and O. Fatibello-Filho, *Anal. Methods*, 2015, **7**, 7568–7573.
63 S. Soares, G. M. Fernandes and F. R. P. Rocha, *TrAC, Trends Anal. Chem.*, 2023, **168**, 117284.
64 T. A. Estrada-Mendoza, D. Willett and G. Chumanov, *J. Phys. Chem. C*, 2020, **124**, 27024–27031.
65 V. B. dos Santos, H. S. de Sousa, R. A. Farias, M. V. Foguel, J. L. de Oliveira and W. T. Suarez, *J. Chem. Educ.*, 2023, **100**, 4488–4495.
66 N. S. Moreira, C. L. S. Chagas, K. A. Oliveira, G. F. Duarte-Junior, F. R. de Souza, M. Santhiago, C. D. Garcia, L. T. Kubota and W. K. T. Coltro, *Anal. Chim. Acta*, 2020, **1119**, 1–10.
67 M. F. Mora, C. D. Garcia, F. Schaumburg, P. A. Kler, C. L. A. Berli, M. Hashimoto and E. Carrilho, *Anal. Chem.*, 2019, **91**, 8298–8303.
68 K. M. Clark, L. Skrajewski, T. E. Benavidez, L. F. Mendes, E. L. Bastos, F. A. Dörr, R. Sachdeva, A. A. Ogale, T. R. L. C. Paixão and C. D. Garcia, *Soft Matter*, 2020, **16**, 7659–7666.
69 Y. Shen, Y. Wei, C. Zhu, J. Cao and D.-M. Han, *Coord. Chem. Rev.*, 2022, **458**, 214442.
70 E. K. N. da Silva, V. B. dos Santos, I. S. Resque, C. A. Neves, S. G. C. Moreira, M. d. O. K. Franco and W. T. Suarez, *Microchem. J.*, 2020, **157**, 104986.
71 C. Yuan, M. Wang, M. Li, P. Sun, R. Gao and J. Tang, *ACS Sustainable Chem. Eng.*, 2022, **10**, 14294–14308.
72 H. Ehtesabi, A. Asadollahi, Z. Hallaji, M. Goudarzi and A. Rezaei, *Sens. Actuators, A*, 2021, **332**, 113057.
73 S. Tang, D. Chen, G. Guo, X. Li, C. Wang, T. Li and G. Wang, *Sci. Total Environ.*, 2022, **825**, 153913.
74 S. Patel, K. Shrivas, D. Sinha, I. Karbhal, T. K. Patle, J. Monisha and S. J. Tikeshwari, *Spectrochim. Acta, Part A*, 2023, **299**, 122824.
75 Y. Ye, T. Wu, X. Jiang, J. Cao, X. Ling, Q. Mei, H. Chen, D. Han, J.-J. Xu and Y. Shen, *ACS Appl. Mater. Interfaces*, 2020, **12**, 14552–14562.
76 W. Silva Lyra, V. B. dos Santos, A. G. G. Dionízio, V. L. Martins, L. F. Almeida, E. Nóbrega Gaião, P. H. G. D. Diniz, E. C. Silva and M. C. U. Araújo, *Talanta*, 2009, **77**, 1584–1589.
77 H. Colzani, Q. E. A. G. Rodrigues, C. Fogaça, J. M. L. N. Gelinski, E. R. Pereira-Filho and E. M. Borges, *Quim. Nova*, 2017, **40**, 833–839.
78 Y. Suzuki, M. Endo, J. Jin, K. Iwase and M. Iwatsuki, *Anal. Sci.*, 2006, **22**, 411–414.
79 J. Yue, H. Feng, X. Jin, H. Yuan, Z. Li, C. Zhou, G. Yang and Q. Tian, *Remote Sens.*, 2018, **10**, 1138.
80 M. B. Stuart, L. R. Stanger, M. J. Hobbs, T. D. Pering, D. Thio, A. J. S. McGonigle and J. R. Willmott, *Sensors*, 2020, **20**, 3293.
81 F. C. Böck, G. A. Helfer, A. B. da Costa, M. B. Dessuy and M. F. Ferrão, *J. Chemom.*, 2020, **34**, e3251.
82 M. E. M. Haertel, E. J. Linhares and A. L. de Melo, *WIREs Forensic Sci.*, 2021, **3**, e1410.
83 X. Tong, G. Cai, Y. Zhu, C. Tong, F. Wang, Y. Guo and S. Shi, *New J. Chem.*, 2022, **46**, 8195–8202.
84 H. S. de Sousa, R. Arruda-Santos, E. Zanardi-Lamardo, W. T. Suarez, J. L. de Oliveira, R. A. Farias and V. Bezerra dos Santos, *Anal. Methods*, 2024, **16**, 2009–2018.
85 I. S. Resque, V. B. dos Santos and W. T. Suarez, *Chem. Pap.*, 2019, **73**, 1659–1668.
86 R. Monošík, V. Bezerra dos Santos and L. Angnes, *Anal. Methods*, 2015, **7**, 8177–8184.
87 C. T. Gee, E. Kehoe, W. C. K. Pomerantz and R. L. Penn, *J. Chem. Educ.*, 2017, **94**, 941–945.
88 B. Gross, S. Y. Lockwood and D. M. Spence, *Anal. Chem.*, 2017, **89**, 57–70.
89 L. Ding, D. Peng, R. Wang and Q. Li, *J. Alloys Compd.*, 2021, **856**, 158160.
90 3D Printing in Analytical Chemistry, *Sample Preparation, Separation, and Sensing*, ed. J. M. H. Martínez, M. Miró, E. J. Carrasco-Correa and M. Vergara-Barberán, Elsevier, 2025.
91 S. Chu, H. Wang, Y. Du, F. Yang, L. Yang and C. Jiang, *ACS Sustainable Chem. Eng.*, 2020, **8**, 8175–8183.
92 C. Mela and Y. Liu, *Appl. Opt.*, 2019, **58**, 8237–8246.
93 M. de Oliveira Krambeck Franco, G. A. Dias Castro, C. Vilanculo, S. A. Fernandes and W. T. Suarez, *Anal. Chim. Acta*, 2021, **1177**, 338844.

94 G. M. Durán, T. E. Benavidez, Á. Ríos and C. D. García, *Microchim. Acta*, 2016, **183**, 611–616.
95 P. Didpinrum, W. Siriangkhawut, K. Ponhong, P. Chantiratikul and K. Grudpan, *RSC Adv.*, 2021, **11**, 36494–36501.
96 X. Li, L. Pan, F. Yang and L. Yang, *ACS Appl. Nano Mater.*, 2022, **5**, 9252–9259.
97 F. Pena-Pereira, W. Wojnowski and M. Tobiszewski, *Anal. Chem.*, 2020, **92**, 10076–10082.
A. H. Alshatteri and K. M. Omer, *Anal. Methods*, 2022, **14**, 1730–1738.
99 V. B. d. Santos, W. M. S. d. Oliveira, J. P. B. d. Almeida, M. V. Foguel, W. T. Suarez and J. L. d. Oliveira, *Quim. Nova*, 2023, **46**(9), 924–930.
100 P. Itterheimová, F. Foret and P. Kubáň, *Anal. Chim. Acta*, 2021, **1153**, 338294.
101 J. Shin and H.-K. Choi, *J. Anal. Sci. Technol.*, 2022, **13**, 44.
102 E. T. da Costa, M. F. Mora, P. A. Willis, C. L. do Lago, H. Jiao and C. D. Garcia, *Electrophoresis*, 2014, **35**, 2370–2377.
103 L. B. Ayres, F. S. Lopes, C. D. Garcia and I. G. R. Gutz, *Anal. Methods*, 2020, **12**, 4109–4115.
104 F. C. Böck, G. A. Helfer, A. B. da Costa, M. B. Dessuy and M. F. Ferrão, *Food Chem.*, 2022, **367**, 130669.
105 H. de Souza Ramos Pontes Moura, A. R. Mól, T. R. Sampaio and A. Fonseca, *Anal. Methods*, 2018, **10**, 5571–5576.
106 I. S. A. Porto, J. H. Santos Neto, L. O. dos Santos, A. A. Gomes and S. L. C. Ferreira, *Microchem. J.*, 2019, **149**, 104031.
107 A. A. Mohamed and A. A. Shalaby, *Food Chem.*, 2019, **274**, 360–367.
108 M. L. Firdaus, W. Alwi, F. Trinoveldi, I. Rahayu, L. Rahmidar and K. Warsito, *Procedia Environ. Sci.*, 2014, **20**, 298–304.
109 M. Wu, T. Liu, C. Yin, X. Jiang, Q. Sun, L. Gao, N. Niu, L. Chen and H. Gang, *Microchem. J.*, 2023, **190**, 108686.
110 P. Magnan, *Nucl. Instrum. Methods Phys. Res., Sect. A*, 2003, **504**, 199–212.
111 T. Hirayama, *IEEE Asian Solid-State Circuits Conference (A-SSCC)*, 2013.
112 P. Korus, *Digit. Signal Process.*, 2017, **71**, 1–26.
113 L. Frey, P. Parrein, J. Raby, C. Pellé, D. Hérault, M. Marty and J. Michailos, *Opt. Express*, 2011, **19**, 13073–13080.
114 P. Xia, S. Wang, F. Gong, W. Cao and Y. Zhao, *J. Build. Eng.*, 2024, **84**, 108633.
115 L. F. Capitán-Vallvey, N. López-Ruiz, A. Martínez-Olmos, M. M. Erenas and A. J. Palma, *Anal. Chim. Acta*, 2015, **899**, 23–56.
116 C. Bennett, P. Sookwong, J. Jakmunee and S. Mahatheeranont, *Anal. Methods*, 2021, **13**, 3348–3358.
117 S. Wang, Y. Ding, L. Zhang, Y. Cheng, Y. Deng, Q. Jiang, H. Gao, J. Gu, G. Yang, L. Zhu, T. Yan, Q. Zhang and J. Ye, *J. Hazard. Mater.*, 2023, **445**, 130563.
118 H. Liang, Y. Li, B. Lin, Y. Yu, Y. Wang, L. Zhang, Y. Cao and M. Guo, *Microchem. J.*, 2022, **175**, 107221.
119 R. C. Gonzalez and R. E. Woods, *Digital Image Processing*, Prentice-Hall, Inc., 3rd edn, 2006.
120 E. Evans, E. F. Moreira Gabriel, T. E. Benavidez, W. K. Tomazelli Coltro and C. D. Garcia, *Analyst*, 2014, **139**, 5560–5567.
121 S. A. Bhakta, R. Borba, M. Taba, C. D. Garcia and E. Carrilho, *Anal. Chim. Acta*, 2014, **809**, 117–122.
122 M. d. O. K. Franco, W. T. Suarez, V. B. dos Santos, I. S. Resque, M. H. dos Santos and L. F. Capitán-Vallvey, *Spectrochim. Acta, Part A*, 2021, **253**, 119580.
123 L. Han, T. Liu, D. Cui, J. Yi, W. Jiang, X. Li, N. Niu and L. Chen, *Spectrochim. Acta, Part A*, 2022, **280**, 121562.
124 K. Moodley and H. Murrell, *Comput. Geosci.*, 2004, **30**, 609–618.
125 S. Šafranko, P. Živković, A. Stanković, M. Medvidović-Kosanović, A. Széchenyi and S. Jokić, *J. Chem. Educ.*, 2019, **96**, 1928–1937.
126 S. A. Nogueira, L. R. Sousa, N. K. L. Silva, P. H. F. Rodrigues and W. K. T. Coltro, *Micromachines*, 2017, **8**, 139.
127 L. von Mühlen, O. D. Prestes, M. F. Ferrão and C. Sirtori, *Molecules*, 2022, **27**, 4721.
128 K. Danzer and L. A. Currie, *Pure Appl. Chem.*, 1998, **70**, 993–1014.
129 E. HRN, HZN - Croatian Standards Institute, International Organisation for Standardisation and Croatian Standard Institute, Zagreb, Croatia, 2007.
130 I. Taverniers, M. De Loose and E. Van Bockstaele, *Trac. Trends Anal. Chem.*, 2004, **23**, 535–552.
131 M. Thompson, S. L. R. Ellison and R. Wood, *Pure Appl. Chem.*, 2002, **74**, 835–855.
132 J. Aitchison and I. R. Dunsmore, *Statistical Prediction Analysis*, Cambridge University Press, 1975.
133 L. A. Currie, *Anal. Chim. Acta*, 1999, **391**, 105–126.
134 L. A. Currie, *Pure Appl. Chem.*, 1995, **67**, 1699–1723.
135 Analytical Methods Committee, *Analyst*, 1994, **119**, 2363–2366.
136 J. K. Taylor, *Anal. Chem.*, 1983, **55**, 600A–608A.
137 M. Feinberg, *J. Chromatogr. A*, 2007, **1158**(1–2), 174–183.
138 N. Gao, P. Huang and F. Wu, *Spectrochim. Acta, Part A*, 2018, **192**, 174–180.
139 S. Wang, X. Bao, B. Gao and M. Li, *Dalton Trans.*, 2019, **48**, 8288–8296.
140 M. Yang, Y. Zhang, M. Cui, Y. Tian, S. Zhang, K. Peng, H. Xu, Z. Liao, H. Wang and J. Chang, *Nanoscale*, 2018, **10**, 15865–15874.
141 X. Qu, Z. Gao, M. Liu, H. zhai, L. Shi, Y. Li and H. Song, *Appl. Surf. Sci.*, 2020, **501**, 144047.
142 K. Faaliyan, H. Abdoos, E. Borhani and S. S. Seyyed Afghahi, *Nanomed. J.*, 2019, **6**, 269–275.
143 K. Shrivas, J. Monisha, S. Patel, S. S. Thakur and R. Shankar, *Lab Chip*, 2020, **20**, 3996–4006.
144 D. Zhang, F. Zhang, S. Wang, S. Hu, Y. Liao, F. Wang and H. Liu, *Spectrochim. Acta, Part A*, 2023, **290**, 122285.
145 X. Zhu, L. Han, H. Liu and B. Sun, *Food Chem.*, 2022, **379**, 132154.
146 M. M. Moghaddam, M. Baghbanzadeh, A. Keilbach and C. O. Kappe, *Nanoscale*, 2012, **4**, 7435–7442.
147 G. Guo, Q. Zheng, T. Li, T. Zhang, S. Tang, L. Li, S. Gao, Y. Tang and D. Chen, *Chem. Eng. Sci.*, 2023, **281**, 119201.

148 H. Guo, R. Yang, D. Lei, X. Ma, D. Zhang, P. Li, J. Wang, L. Zhou and W. Kong, *Microchem. J.*, 2023, **190**, 108586.
149 I. Milenkovic, M. Algarra, C. Alcoholado, M. Cifuentes, J. M. Lázaro-Martínez, E. Rodríguez-Castellón, D. Mutavdžić, K. Radotić and T. J. Bandosz, *Carbon*, 2019, **144**, 791–797.
150 X. Wang, L. Kong, S. Zhou, T. Liang, H. Wan and P. Wang, *J. Electrochem. Soc.*, 2020, **167**, 147520.
151 W. R. Algar, K. Susumu, J. B. Delehanty and I. L. Medintz, *Anal. Chem.*, 2011, **83**, 8826–8837.
152 D. D. Drozd, N. A. Byzova, P. S. Pidenko, D. V. Tsyupka, P. D. Strokin, O. A. Goryacheva, A. V. Zherdev, I. Y. Goryacheva and B. B. Dzantiev, *Anal. Chim. Acta*, 2022, **414**, 4471–4480.
153 G. Guo, T. Li, Z. Liu, X. Luo, T. Zhang, S. Tang, X. Wang and D. Chen, *Food Chem.*, 2024, **432**, 137232.
154 H. M. Kashani, T. Madrakian, A. Afkhami, F. Mahjoubi and M. A. Moosavi, *Mater. Sci. Eng., B*, 2019, **251**, 114452.
155 Y. Sun, M. Wei, R. Liu, H. Wang, H. Li, Q. Kang and D. Shen, *Talanta*, 2019, **194**, 452–460.
156 Y.-P. Sun, B. Zhou, Y. Lin, W. Wang, K. A. S. Fernando, P. Pathak, M. J. Meziani, B. A. Harruff, X. Wang, H. Wang, P. G. Luo, H. Yang, M. E. Kose, B. Chen, L. M. Veca and S.-Y. Xie, *J. Am. Chem. Soc.*, 2006, **128**, 7756–7757.
157 C. Li, X. Xu, F. Wang, Y. Zhao, Y. Shi, X. Zhao and J. Liu, *Food Chem.*, 2023, **402**, 134222.
158 I. Ortiz-Gómez, V. Toral-López, F. J. Romero, I. de Orbe-Payá, A. García, N. Rodríguez, L. F. Capitán-Vallvey, D. P. Morales and A. Salinas-Castillo, *Sens. Actuators, B*, 2021, **332**, 129506.
159 Y. He, Y. Su, X. Yang, Z. Kang, T. Xu, R. Zhang, C. Fan and S.-T. Lee, *J. Am. Chem. Soc.*, 2009, **131**, 4434–4438.
160 X. Zhang, H. Xie, Z. Liu, C. Tan, Z. Luo, H. Li, J. Lin, L. Sun, W. Chen, Z. Xu, L. Xie, W. Huang and H. Zhang, *Angew. Chem., Int. Ed.*, 2015, **54**, 3653–3657.
161 S. Li, D. Chen, F. Zheng, H. Zhou, S. Jiang and Y. Wu, *Adv. Funct. Mater.*, 2014, **24**, 7133–7138.
162 M. Rong, Y. Liang, D. Zhao, B. Chen, C. Pan, X. Deng, Y. Chen and J. He, *Sens. Actuators, B*, 2018, **265**, 498–505.
163 D. Sebastian, R. Kala, K. P. Neethu Parvathy and D. P. Savitha, *J. Mater. NanoSci.*, 2021, **56**, 18126–18146.
164 L. Wang, S. Zheng, Z. Cai, F. Wang and C. Li, *Sens. Actuators, B*, 2023, **394**, 134461.
165 P. Anastas and N. Eghbali, *Chem. Soc. Rev.*, 2010, **39**, 301–312.
166 H. Yu, J. F. MacGregor, G. Haarsma and W. Bourg, *Ind. Eng. Chem. Res.*, 2003, **42**, 3036–3044.
167 M. Meenu, C. Kurade, B. C. Neelapu, S. Kalra, H. S. Ramaswamy and Y. Yu, *Trends Food Sci. Technol.*, 2021, **118**, 106–124.
168 Ministério da Agricultura e Pecuária, *Biblioteca de Normas Vinhos e Bebidas*, 2005.
169 The European Copper Institute, *Technical Guide on Metals and Alloys Used as Food Contact*, 2011.
170 G. M. Durán, T. E. Benavidez, A. M. Contento, A. Ríos and C. D. García, *J. Pharm. Anal.*, 2017, **7**, 324–331.
171 M. Chowdhury, D. Basu and P. K. Das, *Sens. Diagn.*, 2024, **3**, 1329–1343.
172 G.-T. Xu, T.-S. Zhao, K. Zhang, L.-Z. Guo, Y.-Q. He, J.-H. Hu, Y.-J. Liao, X. Mai and N. Li, *Chin. J. Anal. Chem.*, 2023, **51**, 100206.
173 J. Jia, H. Wang, R. Quan, S. Shuang, Z. Wu and S. Li, *Mater. Today Chem.*, 2023, **33**, 101730.
174 Codex Alimentarius, *Codex Pesticides Residues in Food Online Database*, 2024.
175 Food and Agriculture Organization of the United Nations, *Maximum Residue Limits*, 2024.
176 X. Hu, J. Shi, Y. Shi, X. Zou, M. Arslan, W. Zhang, X. Huang, Z. Li and Y. Xu, *Food Chem.*, 2019, **272**, 58–65.
177 L. Xie, X. Zi, H. Zeng, J. Sun, L. Xu and S. Chen, *Anal. Chim. Acta*, 2019, **1053**, 131–138.
178 B. Peng, Y. Guo, Y. Ma, M. Zhou, Y. Zhao, J. Wang and Y. Fang, *Microchem. J.*, 2022, **175**, 107185.
179 C.-X. Yao, L. Yang, J. Wang, H. Lv, X.-M. Ji, S.-J. Li, J.-M. Liu and S. Wang, *Microchim. Acta*, 2022, **189**, 354.
180 Z. Lu, S. Chen, M. Chen, H. Ma, T. Wang, T. Liu, J. Yin, M. Sun, C. Wu, G. Su, X. Dai, X. Wang, Y. Wang, H. Yin, X. Zhou, Y. Shen and H. Rao, *Chem. Eng. Sci.*, 2023, **454**, 140492.
181 G. Guo, T. Li, Q. Zheng, S. Tang, H. Hu, X. Wang and D. Chen, *Sens. Actuators, B*, 2023, **395**, 134523.
182 X. Wang, Y. Yuan, Y. Sun, X. Liu, M. Ma, R. Zhang and F. Shi, *RSC Adv.*, 2022, **12**, 27199–27205.
183 C. Wu, T. Zhou, Z. Gao, M. Li, Q. Zhou and W. Zhao, *Microchem. J.*, 2023, **194**, 109283.
184 N. Lee, C. Wang and J. Park, *RSC Adv.*, 2018, **8**, 22991–22997.
185 C. Dejous and U. M. Krishnan, *Biosens. Bioelectron.*, 2021, **173**, 112790.
186 T. Liu, S. Zhang, W. Liu, S. Zhao, Z. Lu, Y. Wang, G. Wang, P. Zou, X. Wang, Q. Zhao and H. Rao, *Sens. Actuators, B*, 2020, **305**, 127524.
187 R. Bandi, M. Alle, C.-W. Park, S.-Y. Han, G.-J. Kwon, N.-H. Kim, J.-C. Kim and S.-H. Lee, *Sens. Actuators, B*, 2021, **330**, 129330.
188 Y. Ren, L. Cao, X. Zhang, R. Jiao, D. Ou, Y. Wang, D. Zhang, Y. Shen, N. Ling and Y. Ye, *Food Control*, 2023, **145**, 109412.
189 W. Lu, Y. Guo, Y. Yue, J. Zhang, L. Fan, F. Li, Y. Zhao, C. Dong and S. Shuang, *Chem. Eng. Sci.*, 2023, **468**, 143615.
190 X. Cui, T. Lei, J. Zhang, Z. Chen, H. Luo, H. Chen, Y. He and G. Song, *Spectrochim. Acta, Part A*, 2022, **283**, 121727.
191 S. Banerjee and P. Das, *Sens. Actuators, B*, 2024, **401**, 135002.
192 H.-T. Cao, T. Zhao, W. Liu, C.-Y. Xu, Y.-J. Liao, X.-L. Yan, X. Mai and N. Li, *Microchem. J.*, 2024, **197**, 109723.
193 A. B. Kujur, M. L. Satnami, Y. Chawre, P. Miri, A. Sinha, R. Nagwanshi, I. Karbhal, K. K. Ghosh, S. Pervez and M. K. Deb, *RSC Adv.*, 2024, **14**, 20093–20104.
194 R. C. Castro, R. N. M. J. Páscoa, M. L. M. F. S. Saraiva, J. L. M. Santos and D. S. M. Ribeiro, *Spectrochim. Acta, Part A*, 2022, **267**, 120592.
195 Y. Meng, Q. Guo, Y. Jiao, P. Lei, S. Shuang and C. Dong, *Mater. Today Chem.*, 2022, **26**, 101170.

196 G. J. C. Pimentel, L. B. Ayres, J. N. Y. Costa, W. J. Paschoalino, K. Whitehead, L. T. Kubota, M. H. de Oliveira Piazzetta, A. L. Gobbi, F. M. Shimizu, C. D. Garcia and R. S. Lima, *ACS Appl. Mater. Interfaces*, 2024, DOI: 10.1021/acsami.4c01159.
197 S. Wang, Y. Wang, Y. Ning, W. Wang and Q. Liu, *Talanta*, 2024, **271**, 125679.
198 A. Hemmati, H. Emadi and S. R. Nabavi, *ACS Omega*, 2023, **8**, 20987–20999.
199 Z. Shen, C. Zhang, X. Yu, J. Li, Z. Wang, Z. Zhang and B. Liu, *J. Mater. Chem. C*, 2018, **6**, 9636–9641.
200 L. Jia, Z. Xu, R. Chen, X. Chen and J. Xu, *Nanomaterials*, 2022, **12**, 128.
201 N. Azizi, T. Hallaj and N. Samadi, *Luminescence*, 2022, **37**, 153–160.
202 S. Swain, A. K. Jena and T. Mohanta, *ACS Appl. Opt. Mater.*, 2023, **1**, 1236–1244.
203 D. Wei, Y. Wang, N. Zhu, J. Xiao, X. Li, T. Xu, X. Hu, Z. Zhang and D. Yin, *ACS Appl. Mater. Interfaces*, 2021, **13**, 48643–48652.
204 W. Wei, J. Huang, W. Gao, X. Lu and X. Shi, *Chemosensors*, 2021, **9**, 25.
205 X. Wang and T. Wu, *Sci. Total Environ.*, 2023, **879**, 163166.
206 M. S. Giroux, Z. Zahra, O. A. Salawu, R. M. Burgess, K. T. Ho and A. S. Adeleye, *Environ. Sci.:Nano*, 2022, **9**, 867–910.
207 J. Sanmartín-Matalobos, P. Bermejo-Barrera, M. Aboal-Somoza, M. Fondo, A. M. García-Deibe, J. Corredoira-Vázquez and Y. Alves-Iglesias, *Nanomaterials*, 2022, **12**, 2501.
208 X. Wang, Y. Lv, X. Kong, Z. Ding, X. Cheng, Z. Liu and G.-C. Han, *New J. Chem.*, 2023, **47**, 10696–10705.
209 E. C. N. Rezende, F. M. Carneiro, J. B. de Moraes and I. J. Wastowski, *Environ. Sci. Pollut. Res.*, 2021, **28**, 56432–56448.
210 D. Wang, G. Yang, X. Yun, T. Luo, H. Guo, L. Pan, W. Du, Y. Wang, Q. Wang, P. Wang, Q. Zhang, Y. Li and N. Lin, *Environ. Sci. Technol.*, 2024, **17**, 100301.
211 S. Barathi, N. Sabapathi, S. Kandasamy and J. Lee, *Environ. Res.*, 2024, **240**, 117432.
212 P. Das, S. Biswas, S. S. Bhattacharya and P. Nath, *ACS Appl. Nano Mater.*, 2022, **5**, 3265–3274.
213 Y. Zhao, X. Ruan, Y. Song, J. N. Smith, N. Vasylieva, B. D. Hammock, Y. Lin and D. Du, *Anal. Chem.*, 2021, **93**, 13658–13666.
214 R. El-Shaheny, S. Yoshida and T. Fuchigami, *Microchem. J.*, 2020, **158**, 105241.
215 L. Li, C. Yang, Y. Li, Y. Nie and X. Tian, *J. Mater. NanoSci.*, 2021, **56**, 4782–4796.
216 F. Nazir, M. Asad, L. Fatima, A. Bokhari, S. Majeed, B. Fatima, A. A. A. Mohammed and R. R. Karri, *Environ. Res.*, 2023, **231**, 116147.
217 S. H. Al-Jaf and K. M. Omer, *Int. J. Environ. Anal. Chem.*, 2022, **104**, 5773–5786.
218 T. Liu, L. Fu, C. Yin, M. Wu, L. Chen and N. Niu, *Microchem. J.*, 2022, **174**, 107016.
219 J. Zhang, J. Qian, Q. Mei, L. Yang, L. He, S. Liu, C. Zhang and K. Zhang, *Biosens. Bioelectron.*, 2019, **128**, 61–67.
220 B. Chen, J. Ma, T. Yang, L. Chen, P. F. Gao and C. Z. Huang, *Biosens. Bioelectron.*, 2017, **98**, 36–40.
221 H. Xia, J. Hu, J. Tang, K. Xu, X. Hou and P. Wu, *Sci. Rep.*, 2016, **6**, 36794.
222 D. Uriarte, E. Vidal, A. Canals, C. E. Domini and M. Garrido, *Talanta*, 2021, **229**, 122298.
223 L. Zhao, W. Wang, Y. Wang, H. Li, L. Zhao, N. Wang, Y. Wang, X. Wang and Q. Pu, *J. Hazard. Mater.*, 2021, **417**, 125986.
224 R. Jiang, D. Lin, Q. Zhang, L. Li and L. Yang, *Sens. Actuators, B*, 2022, **350**, 130902.
225 R. Jin, D. Kong, X. Yan, X. Zhao, H. Li, F. Liu, P. Sun, Y. Lin and G. Lu, *ACS Appl. Mater. Interfaces*, 2019, **11**, 27605–27614.
226 A. Kathiravan, A. Gowri, V. Srinivasan, T. A. Smith, M. Ashokkumar and M. Asha Jhonsi, *Analyst*, 2020, **145**, 4532–4539.
227 R. Bandi, H. g. Kannikanti, R. dadigala, B. r. Gangapuram, J. r. Vaidya and V. Guttena, *Opt. Mater.*, 2020, **109**, 110349.
228 D. Zhao, W. Ma and X. Xiao, *Nanomaterials*, 2018, **8**, 612.
229 M. Alonzo, R. Alder, L. Clancy and S. Fu, *WIREs Forensic Sci.*, 2022, **4**, e1461.
230 Y.-T. Yen, Y.-S. Lin, Y.-J. Chang, M.-T. Li, S.-C. Chyueh and H.-T. Chang, *Adv. Mater. Technol.*, 2022, **7**, 2200243.
231 M. Philp and S. Fu, *Drug Test. Anal.*, 2018, **10**, 95–108.
232 T. Otłowski, M. Zalas and B. Gierczyk, *Sci. Rep.*, 2024, **14**, 750.
233 D. J. Klapec, G. Czarnopys and J. Pannuto, *Forensic Sci. Int. Synerg.*, 2020, **2**, 670–700.
234 S. M. Tawfik, M. Sharipov, S. Kakhkhorov, M. R. Elmasry and Y. I. Lee, *Adv. Sci.*, 2019, **6**, 1801467.
235 B. A. Lagasse, L. McCann, T. Kidwell, M. S. Blais and C. D. Garcia, *ACS Omega*, 2020, **5**, 20051–20061.
236 W.-Q. Meng, A. C. Sedgwick, N. Kwon, M. Sun, K. Xiao, X.-P. He, E. V. Anslyn, T. D. James and J. Yoon, *Chem. Soc. Rev.*, 2023, **52**, 601–662.
237 N. Tuccitto, G. Catania, A. Pappalardo and G. Trusso Sfrazzetto, *Chemistry*, 2021, **27**, 13715–13718.
238 Y.-T. Yen, Y.-S. Lin, T.-Y. Chen, S.-C. Chyueh and H.-T. Chang, *R. Soc. Open Sci.*, 2019, **6**, 191017.

